DIVERTOR EXPERIMENTS IN ASDEX

The ASDEX-Team

IPP III/73 October 1981

MAX-PLANCK-INSTITUT FÜR PLASMAPHYSIK

8046 GARCHING BEI MÜNCHEN

MAX-PLANCK-INSTITUT FÜR PLASMAPHYSIK

GARCHING BEI MÜNCHEN

DIVERTOR EXPERIMENTS IN ASDEX

The ASDEX-Team

IPP III/73 October 1981

Die nachstehende Arbeit wurde im Rahmen des Vertrages zwischen dem Max-Planck-Institut für Plasmaphysik und der Europäischen Atomgemeinschaft über die Zusammenarbeit auf dem Gebiete der Plasmaphysik durchgeführt.

IPP III/73

The ASDEX-Team

Divertor Experiments in ASDEX

October 1981

A collection of papers presented at the IAEA Technical Committee Meeting on Divertors and Impurity Control, 6 - 1o July 1981, Garching, FRG (to be published in the proceedings of this conference, edited by M.Keilhacker and U.Daybelge).

Contents:

+) Kernforschungsanlage Jülich

DIVERTOR EXPERIMENTS IN ASDEX

The ASDEX Team
presented by M. Keilhacker

Max-Planck-Institut für Plasmaphysik
EURATOM-Association, D-8046 Garching

I. INTRODUCTION - MACHINE AND OPERATIONAL CHARACTERISTICS

ASDEX is a large tokamak characterized by R = 1,65 m, a = 0.40 m, $B_t(R)$ = 2.8 T and I_p = 500 kA. It has two special features: a poloidal divertor and a technical capability for long pulse operation (up to 10 s). Its main goal is to develop techniques for impurity control, recycling control and ash removal in hot plasmas that can be extrapolated to future devices and a reactor.

The technical outlay of ASDEX is described in /1/. The divertor coil triplets with zero net current - and therefore short-range magnetic fields - produce diverted plasmas with almost circular cross-section (see Fig. 1). A poloidal limiter consisting of two halves that can be independently retracted between shots allows limiter (L) and divertor (D) discharges of equal plasma size and cross-section to be compared. By evaporating titanium onto large getter panels placed inside the divertor domes (pumping speed at present $\sim 10^6$ l/s) pumped divertor discharges (DP) can be produced. Plasma current, density

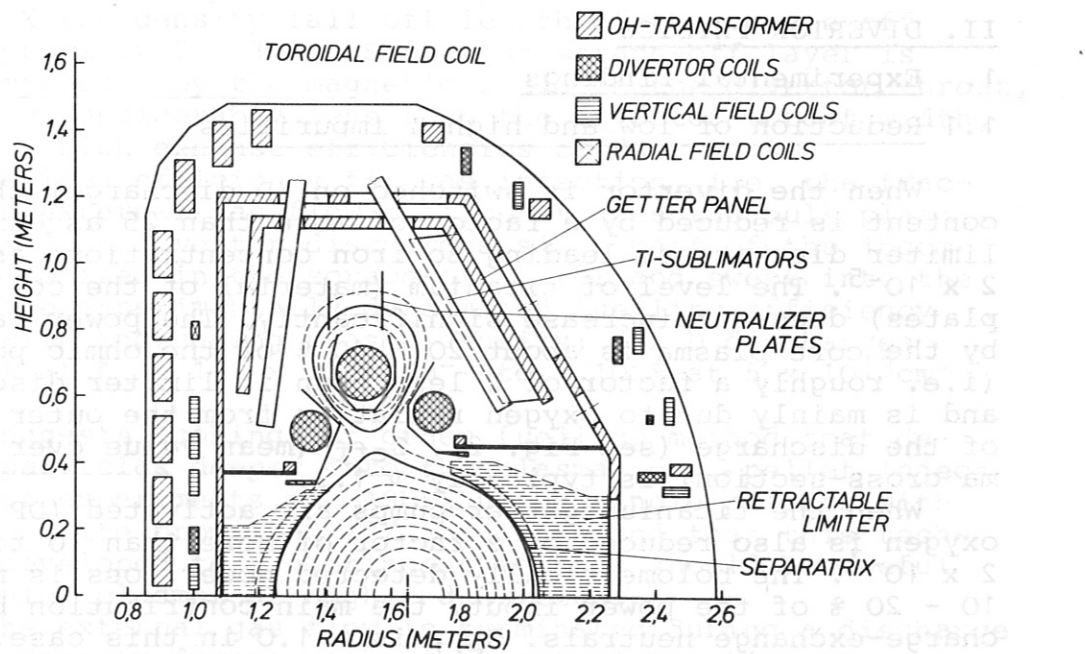

Fig. 1 Simplified cross-section of ASDEX

and position are feedback-controlled to follow a prescribed program.
Diverted ASDEX discharges have a number of favourable characteristics:

- They are highly stable and reproducible.
- No discharge cleaning is necessary, either at the beginning of an experimental day or in between shots.
- The absence of a material limiter allows the plasma column to move (radially) during a disruption, which facilitates disruption control by a feedback system.
- The plasma can be kept very clean ($Z_{eff} \lesssim 1$), even at low densities and for long pulses.
- The plasma parameters can easily be changed, some of them over quite a large range.

Typical parameters of ohmically heated hydrogen plasmas are: $\bar{n}_e = 1 - 7 \times 10^{13}$ cm^{-3}, $T_e \lesssim T_i = 0.5 - 1$ keV, $\tau_E \leq 70$ ms ($\tau_E \sim \bar{n}_e$ up to a critical density) and $q_a = 2.0 - 4.5$.

The possibility of producing reproducible, well controlled plasmas also recommends the divertor as a tool for the study of basic tokamak physics. In this paper we first deal with studies of the divertor itself (experimental findings - part II.1, model of divertor action - part II.2) and then discuss investigations of general tokamak interest for which the divertor only serves as a means for reaching certain experimental conditions (part III). A summary and outlook (part IV) conclude the paper. Some of the topics treated in this review are discussed in more detail in a number of contributed papers to this conference /2, 3, 4, 5, 6/.

II. DIVERTOR PHYSICS

1. Experimental findings

1.1 Reduction of low and high-Z impurities

When the divertor is switched on (D discharge) the iron content is reduced by a factor of more than 25 as compared to limiter discharges, leading to iron concentrations as low as 2×10^{-5}. The level of titanium (material of the collector plates) does not increase significantly. The power radiated by the core plasma is about 20 - 40 % of the ohmic power input (i.e. roughly a factor of 2 less than in limiter discharges) and is mainly due to oxygen radiation from the outer quarter of the discharge (see Fig. 2). Z_{eff} (mean value over the plasma cross-section) is typically ~ 1.3.

When the titanium getter pumps are activated (DP discharges) oxygen is also reduced by a factor of more than 10 to levels of 2×10^{-4}. The bolometrically detected power loss is now down to 10 - 20 % of the power input, the main contribution being from charge-exchange neutrals. Z_{eff} is ~ 1.0 in this case.

In all divertor discharges (D and DP) impurity radiation can be neglected in the central energy balance (see Fig. 2).

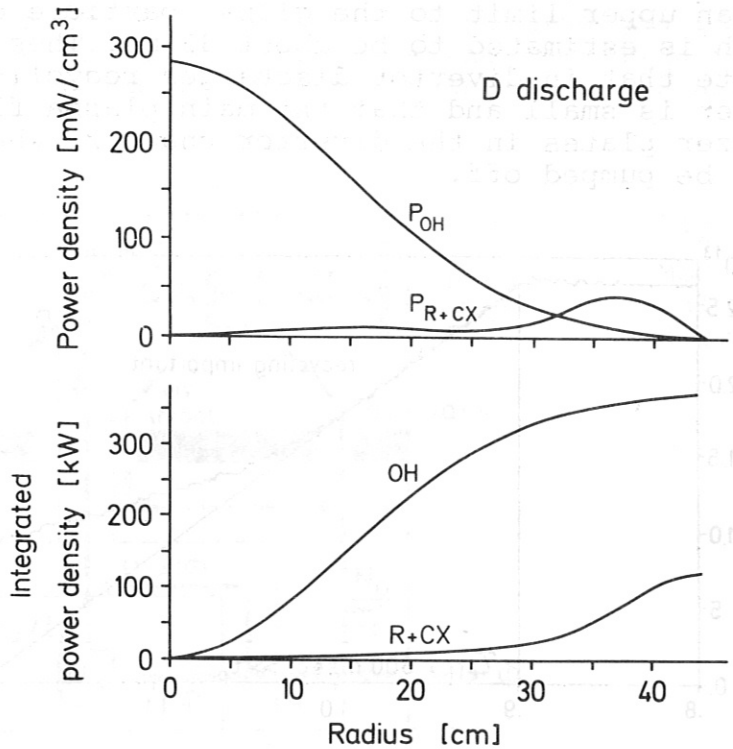

Fig. 2: Radial profiles of ohmic heating power, $P_{OH}(r)$, and total radiation losses, $P_{R+CX}(r)$ (upper part) and corresponding integrated power densities $4\pi^2 R \int_0^r P(r) r dr$ (lower part) for D discharges

1.2 Hydrogen recycling

In ASDEX the density fall-off length of the scrape-off layer is typically 2 - 3 cm. Since the scrape-off layer is further compressed by the magnetic field in the divertor throat, its width is considerably less than the divertor throat width, resulting in high exhaust efficiencies of 80 - 90 %.

The fuelling efficiency for gas injection, i.e. the fraction of the external gas flow that penetrates the bulk plasma, is always < 1 in divertor discharges since part of the incoming gas is ionized in the scrape-off layer and swept into the divertor. The experimentally determined fuelling efficiency decreases with increasing plasma density; for D discharges from $\sim$ 50 % at $\bar{n}_e$ = 1-2 x 10^{13} cm^{-3} to $\sim$ 10 % at 5 x $10^{13} cm^{-3}$ /2/.

This suggests looking for other fuelling method that deposit the particles deeper into the plasma, e.g. pellet injection. Initial experiments on ASDEX using single pellets with 1 mm Ø were quite promising /7/ and indicated that this technique, if developed to a continuous method, should be useful for sustaining plasmas at higher densities.

When the external gas flow is terminated during a discharge the plasma density decays with a characteristic time $\tau_{eff} = \tau_p/(1-r)$, r being the recycling coefficient. At medium densities this decay time is $\sim$ 0.3 s for D and $\sim$ 0.04 s for DP dis-

charges (Fig. 3). The latter value for a pumped divertor discharge puts an upper limit to the global particle confinement time τ_p which is estimated to be about 35 ms. These experiments indicate that in divertor discharges recycling in the plasma chamber is small and that the main plasma flow goes to the neutralizer plates in the divertor chamber, where the neutral gas can be pumped off.

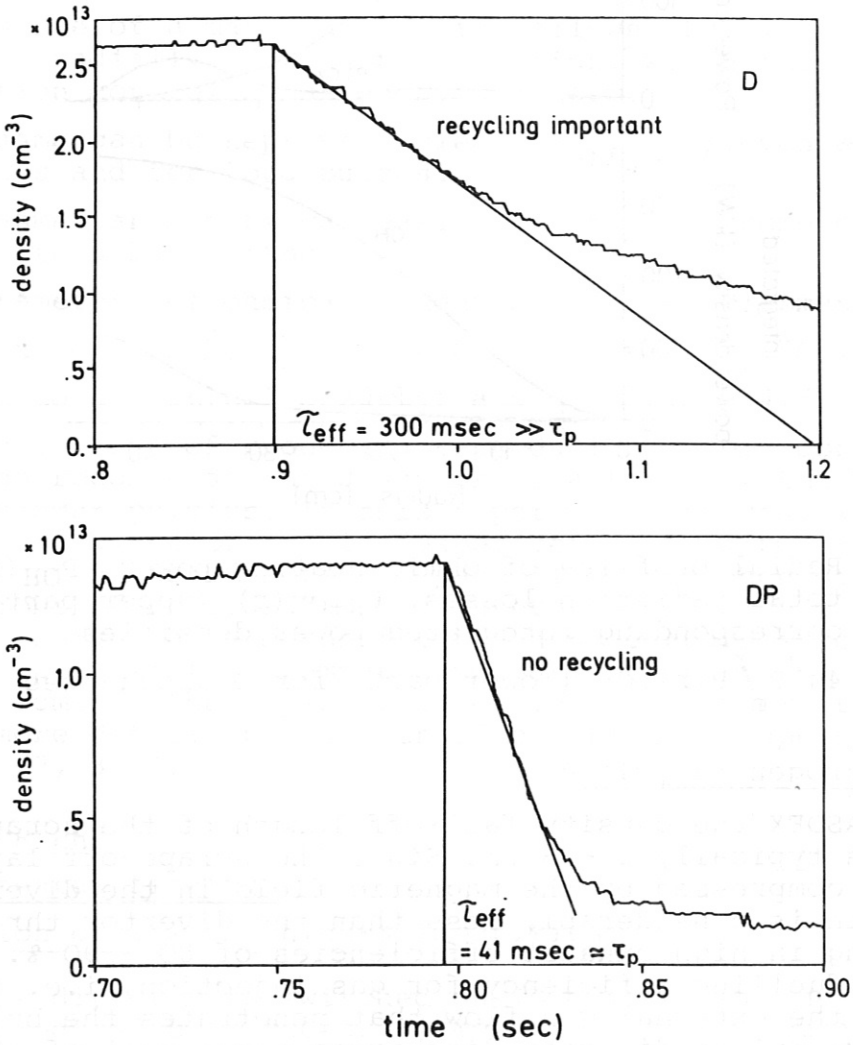

Fig. 3: Decay of plasma density after termination of external gas flow for D and DP discharges.

This leads to a model for global particle balance in divertor discharges as shown schematically in Fig. 4 which can be described by the following equations /2/:

$$\frac{dN_e}{dt} = \gamma\phi - \frac{N_e}{\tau_p} \qquad \text{with } \phi = \phi_G + \frac{N_o}{\tau_c} \ ,$$

$$\frac{dN_o}{dt} = r_p\,\phi_D - \frac{N_o}{\tau_c} - \frac{N_o}{\tau_D} \quad \text{with } \phi_D = (1-\gamma)\,\phi + \frac{N_e}{\tau_p}$$

Here (1-γ) is the fraction of the incoming gas that is ionized in the scrape-off layer and r_p is the recycling coefficient of the collector plates. The other quantities are understandable from Fig. 4.

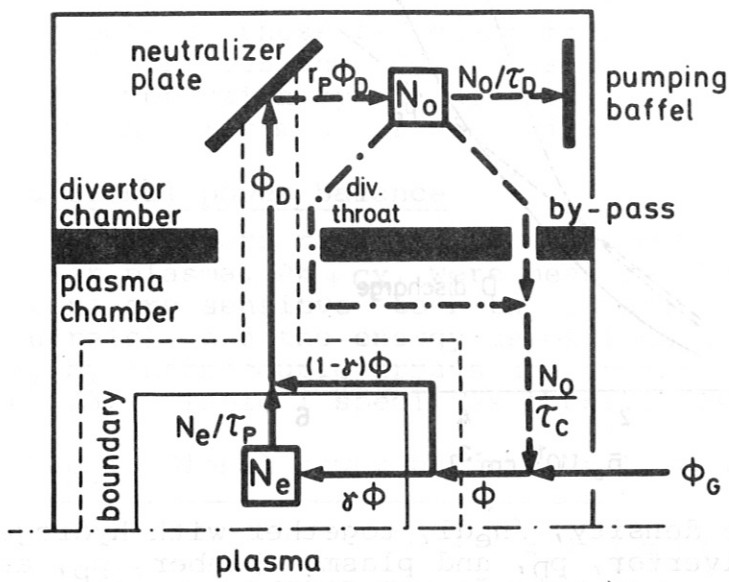

Fig. 4

Model of particle balance in divertor discharges

1.3 Cross-field particle tranpsort

The radial and temporal evolutions of line radiation from different ionization states was measured in the VUV and X-ray regions for impurities such as O and Fe ("natural" impurities), Ne and Ar (injected impurities). The measured distributions are consistent with a numerical model in which the fluxes of all species are described by the simple expression /4/

$$\phi_k = - D \frac{\partial n_k}{\partial r} + v_D \, n_k \, ,$$

in which the anomalous diffusion coefficient D is independent of the radius and has the same numerical value (D = 4000 cm^2/s for medium plasma densities) for all species and $v_D = - \frac{2D}{a^2} \cdot r$ is a convective inward drift.

Measurements on low ionization stages of O indicate that the same diffusion coefficient also holds very close to the separatrix. It also explains the measured width of the scrape-off layer, λ, if one uses the well-known formula $\lambda = (D \cdot \tau_{\parallel})^{1/2}$, where $\tau_{\parallel}$ is the mean confinement time of the plasma in the scrape-off layer and was determined spectroscopically ($\tau_{\parallel}$ = 1-3ms).

1.4 Gas compression in divertor

In Fig. 5 the neutral hydrogen densities and pressures as measured in one of the divertor chambers (P_D) and the plasma chamber (P_p) by quadrupole mass-spectrometers are plotted as functions of the line average plasma density $\bar{n}_e$. The results show a strong build-up of neutral gas pressure in the divertor

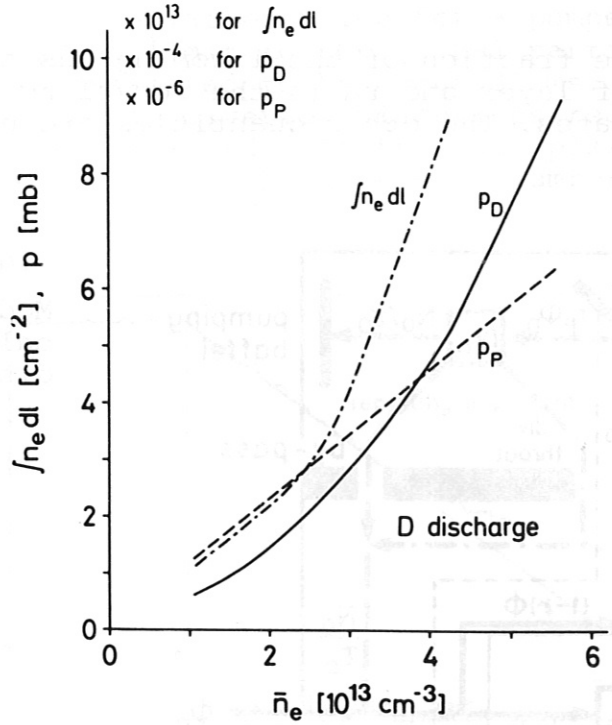

Fig. 5 Scrape-off line density, $\int n_e dl$, together with hydrogen pressures in divertor, p_D, and plasma chamber, p_p, as function of plasma density $\bar{n}_e$.

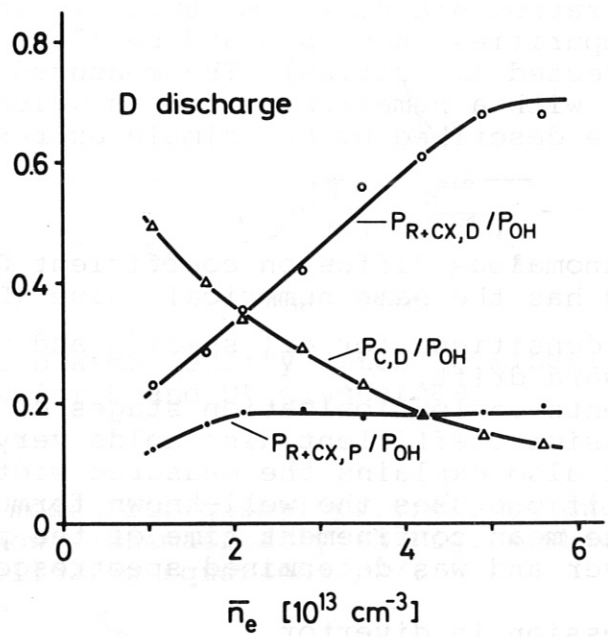

Fig.6 Bolometric powers from core plasma, $P_{R+CX,P}$, and divertor plasma, $P_{R+CX,D}$, together with power on neutralizer plates, $P_{C,D}$, as a function of plasma density $\bar{n}_e$.

region, indicating that the plasma flow into the divertor acts as a diffusion pump. This gas pressure increases non-linearly with the plasma density, reaching 10^{-3} mb ($\hat{=} 5 \times 10^{13} H^{o}/cm^{3}$ at room temperature) at $\bar{n}_e = 6 \times 10^{13}$ cm^{-3}. Also plotted is the line density of the scrape-off layer in the divertor chamber, $\int n_e dl$, which has the same non-linear dependence on $\bar{n}_e$ as the gas pressure, suggesting that there is strong coupling between these two quantities.

Impurities and admixtures of rare gases show roughly the same compression by the divertor as hydrogen, i.e. there is not much enrichment or de-enrichment of these gases.

1.5 Global power balance

The powers radiated from the core plasma and from the divertor plasma, P_{R+CX}, were measured bolometrically (the bolometers are sensitve to both radiation and charge exchange neutrals), and the energy deposition on the neutralizer plates, P_C, by thermocouple arrays and an infrared camera (for details see /3/). Table I specifies these individual quantities for

Table I: Global power balance in L, D and DP discharges

	L	D		DP
	q = 4.4	q = 4.4	q = 2.2	q = 2.2
Power Input P_{OH} (KW)	290	290	540	450
Core Plasma:				
P_{R+CX}/P_{OH}	0.46	0.33	0.22	0.15
Divertor (Limiter):				
P_{R+CX}/P_{OH}	-	0.38	0.40	0.28
P_C/P_{OH}	?	0.20	0.30	0.40

L, D and DP discharges at a plasma density of $\bar{n}_e = 3 \times 10^{13}$ cm^{-3}. Figure 6 shows how the distribution of power onto the different loss channels varies with plasma density $\bar{n}_e$ (D discharge). For this set of data the plasma current was kept constant (I_p = 400 kA) with the ohmic power input P_{OH} increasing with density from 350 kW to 570 kW.

The main conclusions from these measurements are:

- The divertor reduces core radiaton by afactor of about 2 compared with limiter discharges.
- The divertor absorbs 60 - 80 % of the total power input.
- The fraction of this absorbed power that is radiated and charge exchanged in the divertor chamber increases with plasma density, reaching 80 % (or 65 % of the total power input) at $\bar{n}_e = 5 \times 10^{13}$ cm^{-3}. This is the result of the high gas pressures that are observed to build up in the divertor chamber at high plasma densities.
- The overall energy accountability in diverted discharges is rather good (80 - 100 %).

The profiles of energy deposition on the neutralizer plates as measured with the infrared camera show a characteristic width of 1 - 2 cm (at $\bar{n}_e \gtrsim 2 \times 10^{13}$ cm^{-3}).

2. MODEL OF DIVERTOR ACTION

The experimental results discussed in the previous section allow a first picture of divertor action in ASDEX that, apart from minor pecularities which are due to structural details of this divertor design, should apply to poloidal divertors in general.

When the divertor magnetic field configuration is established, particles and energy stream into the divertor in a narrow layer ($\lambda_n \sim$ 2-3 cm, $\lambda_{Te} \sim$ 1.5 cm) outside the separatrix. The width of the density profile $\lambda_n = (D_\perp \tau_\parallel)^{1/2}$ is determined by anomalous diffusion, with a diffusion coefficient $D_\perp$ that has the same value for hydrogen and impurities. The latter fact makes the shielding effect of the scrape-off layer against wall-released impurities small since shielding requires that the ratio of cross-field to parallel transport (with characteristic times $\tau_\perp$ and $\tau_\parallel$) be different for hydrogen (H) and impurities (I):

$$\tau_{\perp I} = \lambda^2 / D_{\perp I} \quad \text{with } \lambda = (D_{\perp H}\, \tau_{\parallel H})^{1/2};$$

$$\frac{\tau_{\perp I}}{\tau_{\parallel I}} = \frac{D_{\perp H}}{D_{\perp I}} \cdot \frac{\tau_{\parallel H}}{\tau_{\parallel I}} \lesssim 1 \quad .$$

$$\sim 1 \qquad \lesssim 1$$

This small shielding efficiency, on the other hand, strongly suggests that the observed reduction of iron content in diverted discharges is due to shifting the plasma-wall contact from the limiter to the neutralizer plates, i.e. a change in the impurity source function, and not to significantly improved impurity screening.

The plasma flow into the divertor brings about a strong build-up of neutral hydrogen in the divertor chambers (compression by a factor of more than 100). Interaction of this gas with the scrape-off plasma affects the density in the scrape-off layer, leading to rather large line densities (2 to 10 x 10^{13} cm^{-2}). Besides, the high gas pressure in the divertor causes the plasma flow into the divertor to be sub-sonic, with constant pressure along the magnetic field lines (spectroscopic measurements show that the flow velocity is about 1/10 of the ion sound velocity $c_s = [2(kT_e+kT_i)/m_i]^{1/2}$).

The large neutral gas pressure in the divertor chamber has two important consequences: Firstly, a remote gas blanket is formed in front of the neutralizer plates in which plasma energy is lost by radiation, charge exchange and enhanced recycling thereby reducing the temperature near the plates to less than 10 eV (cool plasma mantle). Secondly, the high pressure would reduce the requirements on the pumping speed for exhausting the He ash in a reactor.

The resulting temperature gradient favours parallel electron heat conduction as the dominant mechanism for transporting the energy from the plasma edge to the divertor. Because of its strong temperature dependence ($q_\parallel \sim T_e^{7/2}$) parallel heat conduction also limits T_e at the

plasma edge ($T_{es} \sim 20 - 40$ eV from laser light scattering, $T_{is} \sim 50 - 80$ eV from neutral charge exchange measurements) and causes a radial T_e-profile with a rapid decrease close to the separatrix, followed by an extended low temperature tail. Simulation of these processes by the BALDUR transport code with a 1-d scrape-off model /6/ indicates that ~ 80 % of the scrape-off energy losses are due to parallel heat conduction and only ~ 20 % to convection.

The hydrogen cycle in diverted discharges is strongly affected by the scrape-off plasma (c.f. Fig. 4). First the scrape-off layer determines the fuelling efficiency of the external gas flow, then it channels the plasma losses (together with the part of the external gas flow that is ionized in the boundary layer) into the divertor chamber, and finally its efficiency in blocking the divertor throat defines the backflow of neutral hydrogen from the divertor into the main plasma chamber. In diverted ASDEX discharges hydrogen recycling takes place via the divertor chambers: The plasma flows into the divertor and is neutralized at the collector plates. Then part of the neutral gas streams back through the divertor throats (probably "inside" the separatrix, i.e. between separatrix and mid divertor coil casing) and, to a lesser extent, through additional, structurally dependent by-passes. (It should be mentioned that on the basis of the measurements hitherto existing it can not be excluded that part of the recycling may be due to backstreaming of plasma from the divertor). In principle, it should be possible to improve the blocking of the divertor throat by the scrape-off plasma (and thereby possibly further increase the divertor gas pressure) by making the divertor throat width smaller and by keeping the electron temperature of the scrape-off plasma in the divertor throat high enough for ionization.

III. GENERAL TOKAMAK PHYSICS

1. Inside-outside asymmetry of transport

In a double-null poloidal divertor configuration the two scrape-off regions on the small and on the large major radius side of the plasma torus are separated by the two stagnation lines. Measurements of the energy deposition on the neutralizer plates by thermocouple arrays (Fig. 7) and of the scrape-off

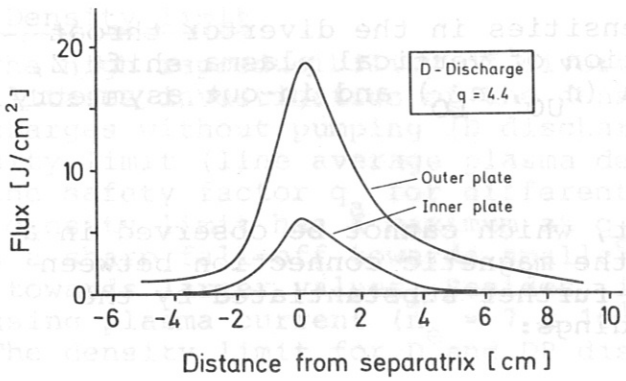

Fig. 7

Energy deposition on outer and inner neutralizer plates (upper divertor)

line density in front of these plates by 8 mm microwave interferometers show that the particle and energy flow into a double-null divertor is about 5 times larger on the outside than on the inside. In contrast, when the configuration is changed into that of a single-null divertor by shifting the plasma vertically towards one of the two divertors the particle and energy flow to the inner and outer neutralizer plates becomes almost equal (approaching ~ 1.25). This is demonstrated in Fig. 8, which displays the line densities in the upper (n_{UO}) and lower (n_{LO}) outside divertor throats - indicating the up-down symmetry of the plasma - and the ratio of the outside to inside divertor throat densities for the upper divertor n_{UO}/n_{UI}, both as functions of the vertical plasma shift Z. The vertical plasma shift necessary to produce a single-null divertor configuration ($\Delta Z \sim 2$ cm) is roughly equal to the width of the scrape-off layer.

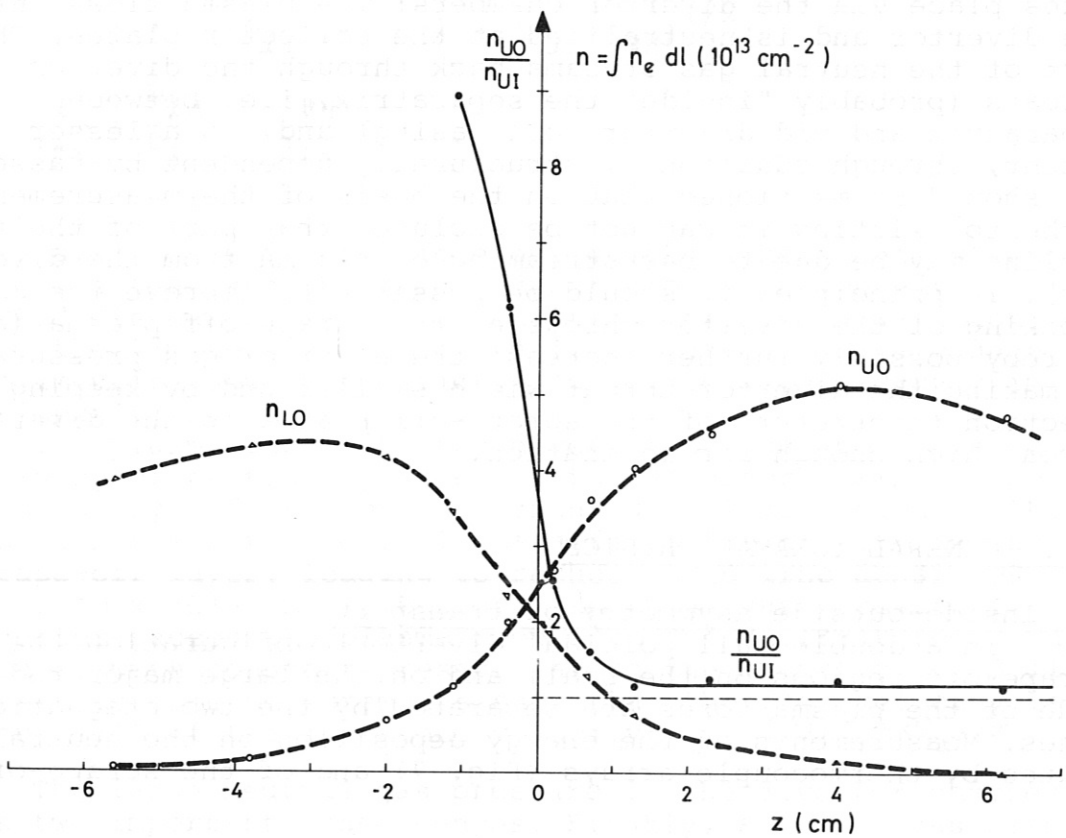

Fig. 8 Scrape-off line densities in the divertor throat $n = \int n_e dl$ as function of vertical plasma shift Z, indicating up-down (n_{UO}, n_{LO}) and in-out asymmetry (n_{UO}/n_{UI}).

This asymmetry in transport, which cannot be observed in a normal tokamak because of the magnetic connection between "inside" and "outside", is further substantiated by the following experimental findings:

- Bringing the movable inner limiter (c.f. Fig.1) right up to the separatrix does not change the particle and energy flows to the inner neutralizer plate.
- Variation of the distance between the outer limiter and the separatrix reduces the flow to both the outer and inner neutralizer plates keeping the asymmetry unchanged.
- The charge exchange neutral flux near the limiter increases by more than an order of magnitude if the outside limiter approaches the separatrix but is almost unaffected by the inside limiter (Fig. 9).
- Fuelling the plasma by gas puffing from the inside instead of - as is usual - from the outside does not affect the asymmetry.

Only part of the observed asymmetry can be explained by geometrical effects (about a factor of 2) so that the results are strongly indicative that cross-field particle and energy trnasport is larger at the large major radius side of a plasma torus than at the small one. The reason for this could lie in the fact that the toroidal magnetic field decreases with major radius or in the unfavourable curvature of the toroidal field at the large major radius side of the torus.

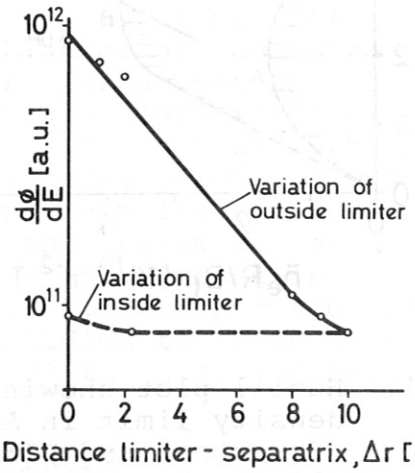

Fig. 9 Variation of charge exchange flux $d\phi/dE$ (at E = 500 eV) at the limiter position with the distance limiter - separatrix, Δr.

2. Density limit

The high reproducibility of diverted ASDEX discharges facilitates investigation of the density limit. For divertor discharges without pumping (D discharges) Fig. 10 displays the density limit (line average plasma density $\bar{n}_e$) as a function of the safety factor q_a for different plasma currents I_p. The density limit has a maximum at q_a values slightly below 3 with a sharp fall-off towards smaller and a less pronounced one towards larger values. Besides, it increases with increasing plasma current ($\bar{n}_e = 7 \times 10^{13}$ cm^{-3} at I_p = 400 kA).

The density limit for D and DP discharges is plotted as

$1/q_a$ versus $\bar{n}_e R/B_t$ (Hugill plot) in Fig. 11 together with corresponding values from DITE (for ohmic heating only). One sees that in this presentation the density limit in diverted ASDEX discharges is considerably higher than that in limiter discharges on DITE.

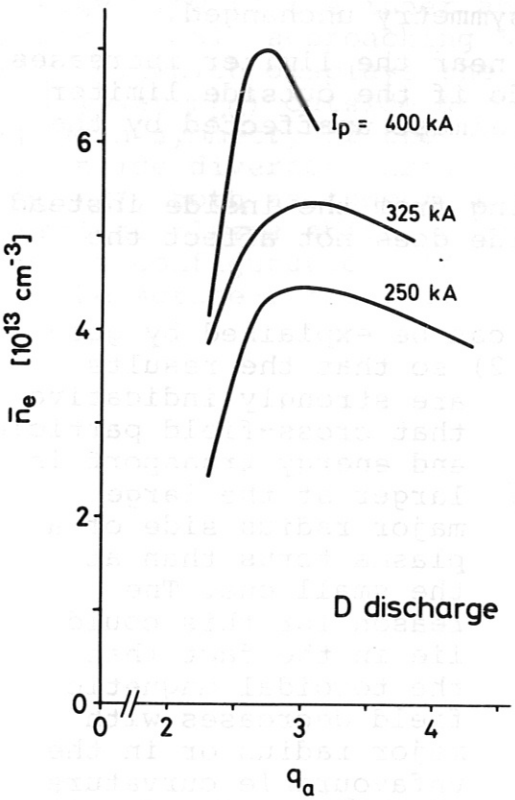

Fig.10 Density limit $\bar{n}_e$ as function of safety factor q_a for D discharges

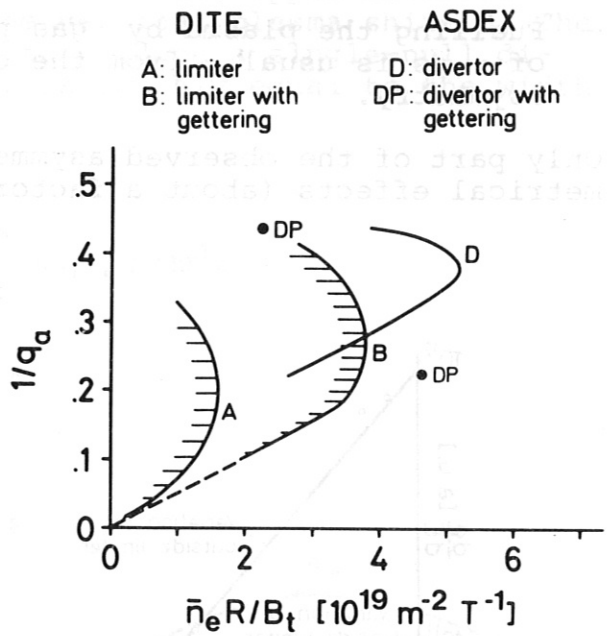

Fig.11 Hugill plot showing the density limit in ASDEX (divertor) and DITE (limiter)

3. Long pulse suprathermal discharges

In standard ASDEX discharges the pulse length is limited to $\sim$ 3 s by the available transformer flux swing. In clean, extremely low density discharges ($\bar{n}_e$ = 1-2 x 10^{12} cm^{-3}) increased plasma conductivity leads to a reduction of the loop voltage by an order of magnitude (from U_L = 1.2 to 0.12 V) and to pulse lengths of more than 10 s that are limited only by the toroidal field power supply. In these experiments, which are produced by closing the gas valve during the plateau phase of a standard DP discharge, the divertor has two important tasks: it prevents plasma pollution for the whole period of 10 s and allows very low density operation by reducing the recycling.

Details of these long suprathermal discharges are discussed in /5/ and /8/. While the distribution functions of electrons and ions show suprathermal tails, runaway electrons in the MeV range are found to disappear with decreasing plasma density.

The experimental findings are consistent with a bulk electron temperature in the range of 1.5 - 3.7 keV. Together with the very low ohmic power input of ∿ 30 kW these temperatures imply an electron energy confinement time of τ_E > 50 ms, which is much larger than predicted by ALCATOR scaling (τ_E ∿ 2 ms). Because of the small number of particles involved this regime appears very attractive for investigations of auxiliary heating and driven currents.

IV. SUMMARY AND OUTLOOK

The ASDEX divertor has been successful in suppressing metal impurities to levels ≤ 2 x 10^{-5}, and in producing clean plasmas with $Z_{eff} \simeq 1$ which could be sustained for several seconds. In some respects the understanding of a poloidal divertor has been modified: The main advantages lie not in the shielding efficiency of the scrape-off layer, but rather in the transfer of plasma-wall contact from the plasma chamber to the divertor, and in the strong gas compression by the divertor which results in high pumping efficiencies. The excellent properties of the poloidal divertor as an energy dump and the possibility of protecting the neutralizer plates by a cold gas blanket are encouraging results in view of the larger power fluxes that have to be handled in future experiments.

In June 1981 the first of two tangential neutral beam lines, with a neutral beam power (into the torus) of 1.25 MW and a pulse length of 0.2 s, was put into operation (the second beam line will follow in the fall of 1981). First injection experiments at a plasma density of $\bar{n}_e$ = 4 x 10^{13} cm^{-3} led to an increase in central ion temperature from 0.5 keV to ∿ 2.2 keV (at I_p = 400 kA). Extension of the previous divertor studies to these higher power fluxes will be the main task of the near future.

REFERENCES

/1/ Keilhacker, M., et al., in: Plasma Physics and Controlled Nuclear Fusion Research 1980, II; International Atomic Energy Agency, Vienna, 1981, p. 351

/2/ Wagner, F., and the ASDEX-Team, Paper I-C4, these proceedings

/3/ Müller, R., and the ASDEX-Team, Paper I-C5, these proceedings

/4/ Engelhardt, W., and the ASDEX-Team, Paper I-C6, these proceedings

/5/ Fußmann, G., and the ASDEX-Team, Paper I-C8, these proceedings

/6/ Becker, G., and Singer, C.E., Paper II-C2, these proceedings

/7/ Büchl, K. and Vlases, G. and the ASDEX-Team, Bull.Am.Phys.Soc.26, 1981, 888

/8/ Fußman, G., et al., Phys.Rev.Lett. 47, 1981, 1004

HYDROGEN RECYCLING IN DIVERTOR DISCHARGES OF ASDEX

The ASDEX Team
presented by F.Wagner

Max-Planck-Institut für Plasmaphysik
EURATOM-Association, D-8046 Garching

Abstract

In limiter discharges protons are recycled effectively at the limiter. In divertor discharges recycling occurs via the divertor chambers. Plasma which is transported into the divertor chambers is neutralized there and backstreams as gaseous hydrogen into the main plasma chamber. The backflow occurs through the divertor necks and through additional openings within the plates which separate divertor chambers and main plasma chamber. There is no substantial recycling at the wall which surround the main plasma or at the divertor necks. The particle balance of a divertor discharge differes from that of a limiter discharge in two important aspects: by the fuelling efficiciency $\gamma < 1$ and by the balance between the main plasma content and the atom content in the divertor chambers. During the stationary phase of a discharge the recycling flux increases in time while the fuelling efficiency decreases.

1. Introduction

Recycling denotes the circular process whereby plasma particles, which leave the plasma and hit the wall, are reemitted from the wall and subsequently reionized within the plasma /1/. This contribution deals with the present status of experiments and our understanding of hydrogen recycling in divertor discharges of ASDEX. Recycling studies of hydrogen in limiter discharges of ASDEX are described in Ref. /2/.

2. Experimental results

If the material limiter is withdrawn from a divertor discharge (D) limited by the magnetic separatrix, the external gas influx Φ_G has to be increased from $6 \cdot 10^{20}$ atoms/sec to $2.3 \cdot 10^{21}$ atoms/sec to maintain a constant electron line density of $2.6 \cdot 10^{13} cm^{-3}$. A further increase in Φ_G up to $7 \cdot 10^{21}$ atoms/sec is required at the transition from a D-discharge to a pumped divertor discharge (DP) when titanium is evaporated within the divertor chamber prior to each discharge.

When the external gas valve is closed during the discharge, the total number of electrons N_e in the plasma decays. At medium density the decay time τ_{eff} is 0.4 sec in a limiter discharge, 0.3 sec in a D-discharge and can be as low as 0.04 sec in a DP-discharge (see Fig. 3 in paper 1.R3).

At the moment when the external gas valve is closed the

slope with which the plasma content N_e decays is N_e/τ_{eff}. N_e/τ_{eff} is the actual influx into a discharge which is switched off by closing the gas valve. In a limiter discharge $N_e/\tau_{eff} \cong \Phi_G$. In Fig. 1 Φ_G and N_e/τ_{eff} are plotted versus the electron line density of D-discharges with different plateau densities: $N_e/\tau_{eff} < \Phi_G$.

3. Conclusions

The following conclusions can be drawn from the experimental results:

- In divertor discharges recycling occurs via the divertor chambers. The conclusion that hydrogen gas backstreams out of the divertor chambers is also supported by Hα-measurements carried out in the main plasma chamber during D-discharges. The Hα-signal shows the same time dependence as the measured gas pressure in the divertor chamber.
- There is recycling in D-discharges ($\tau_{eff} \gg \tau_p$). τ_p is the global particle confinement time and is estimated to be about 35 msec. In DP-discharges, however, $\tau_{eff} \sim \tau_p$. This demonstrates that in divertor-discharges there is no predominant recycling at the walls which surround the main plasma or at the divertor necks. The recycling occurs at the neutralizer plates within the divertor chambers. In D-discharges, hydrogen gas can recycle, in DP-discharges it is pumped.
- Part of the external gas inflow Φ_G is ionized in the boundary layer and carried into the divertor. In divertor discharges the fuelling efficiency $\gamma = N_e/\tau_{eff}/\Phi_G < 1$.

4. Recycling model

These conclusions lead us to the recycling model, shown in Fig. 2. The external gas flux Φ_G together with the recycling flux N_o/τ_c penetrates the plasma. Only the fraction γ compensates the plasma loss N_e/τ_p. The fraction $(1-\gamma)$ of the external and recycling flux together with the plasma loss N_e/τ_p recycle at the neutralizer plate with a recycling coefficient of r_p to give rise to the atom content N_o in the divertor chambers. Atoms in the divertor chambers are lost to the external pumps (N_o/τ_{TP}, which can be neglected), or in the case of DP-discharges into the pumping baffels (N_o/τ_D) and by recycling through by-pass holes in the walls between the main plasma chamber and divertor chambers and through the divertor necks. The global particle balance equations are:

$$\frac{dN_e}{dt} + \frac{N_e}{\tau_p} = \gamma\left(\Phi_G + \frac{N_o}{\tau_c}\right) \qquad (1)$$

$$\frac{dN_o}{dt} = r_p\left[(1-\gamma)\left(\Phi_G + \frac{N_e}{\tau_c}\right) + \frac{N_e}{\tau_p}\right] - \frac{N_o}{\tau_c} - \left[\frac{N_o}{\tau_D}\right] - \left[\frac{N_o}{\tau_{TP}}\right] \qquad (2)$$

The particle balance of a divertor discharge differs from that of a limiter discharge in two important aspects: by the fuelling efficiency $\gamma < 1$ and by the balance between the main plasma content and the atom content in the divertor chambers.

5. Conductance between main plasma chamber and divertor chamber

In order to utilize the recycling equations (1) and (2), the conductance between the divertor and plasma chambers has to be determined. There are two paths for the hydrogen backflow from the divertor.

- through the divertor neck, which, however, may be blocked by the plasma.
- through additional openings (by-pass) in the plates which separate the divertor chambers from the main plasma chamber.

The conductance through the by-pass has been measured and corresponds to τ_c = 44 msec. In order to investigate the possibility and magnitude of backflow through the divertor necks, two sets of experiments were carried out: with the by-pass open and with the by-pass closed. Closing the by-passs has a marginal effect on Φ_G, τ_{eff} or the boundary density, but causes an increase in hydrogen pressure in the divertor chamber by about 50 %. From this observation we have to conclude that the recycling flux occurs predominantly through the divertor neck. From the 50 %-pressure increase which is observed when the by-pass is closed a conductance through the divertor neck corresponding to 22 msec is estimated. The same value is obtained from pressure increase in the divertor chamber which occurs when gas is puffed into one divertor chamber instead of into the main plasma chamber.

Fig. 3 shows photographs of two discharges taken with a red filter so that only Hα-radiation is recorded. Fig. 3a is obtained during a discharge with by-pass open and Fig. 3b during a discharge with the same parameters but with by-pass closed. It is obvious that there is recycling through the divertor neck. Comparison between both pictures shows that the effect of the open by-pass is to spread out the recycling flux over the whole plasma circumference.

Experimental values of Φ_G and N_o together with the estimated values of τ_c and τ_p may be put into eq. (1) and (2) to determine the fuelling coefficient γ and the recycling coefficient r_p of D and DP-discharges.

γ and r_p are plotted in Fig. 4 versus line density. These values are typical; deviations in magnitude occur during a plasma discharge. Although plasma current and line density are kept constant it is found that N_o (and with it the electron boundary density measured in the divertor) increases while Φ_G decreases in time. Values of Φ_G and the recycling flux N_o/τ_c are shown in Fig. 5b and compared with the plasma loss flux N_e/τ_p during the stationary phase of the discharge. Fig. 5c shows the corresponding values for γ and r_p.

6. Comments

The results presented above may change in detail in case the conductance through the divertor neck is not a constant but depends on plasma parameters. Up to now there is no experimental evidence for this.

At high pressure in the divertor chamber, plasma recycling may no longer occur at the neutralizer plate. Charge exchange measurements in the divertor chamber reveal a distinct peak

of backreflected atoms at the intersection of the separatrix and the neutralizer plate. This peak disappears for plasma densities > 5 · $10^{13}cm^{-3}$.

References

/1/ E.S. Marmar, J. Nucl. Mater. 76/77 (1978)59.
H.C. Howe, J. Nucl. Mater., 93/94 (1980)17.

/2/ F. Wagner, "Investigation of Limiter Recycling in the Divertor Tokamak ASDEX", IPP III/71, Garching, W. Germany 1981.

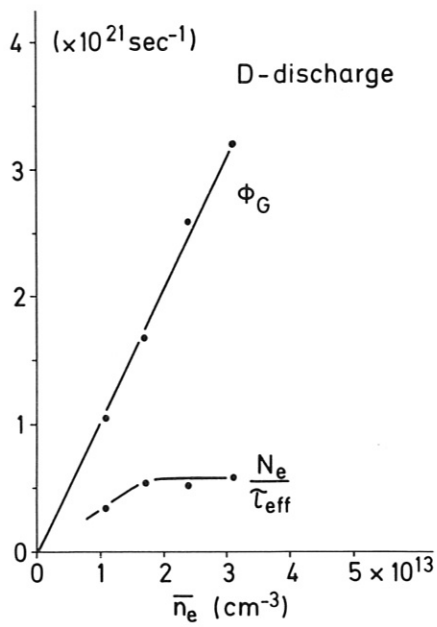

Fig.1
External gas input ϕ_G and decay rate of plasma content N_e/τ_{eff} versus electron density $\bar{n}_e$.

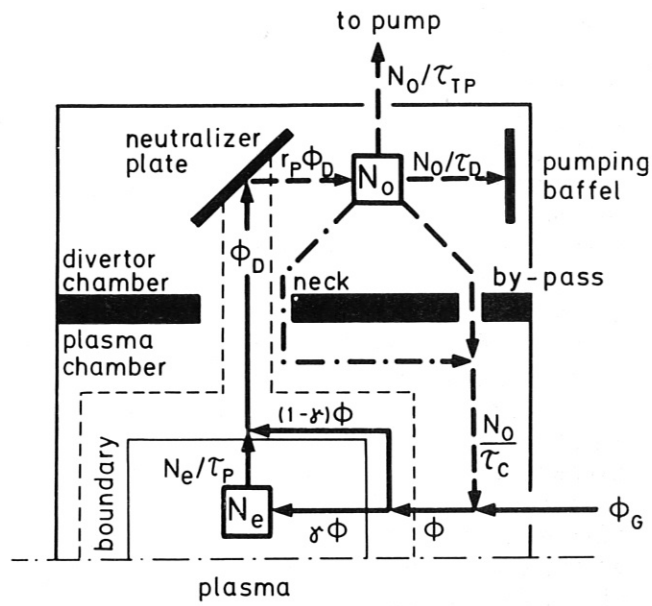

Fig.2
Recycling model of a divertor discharge.

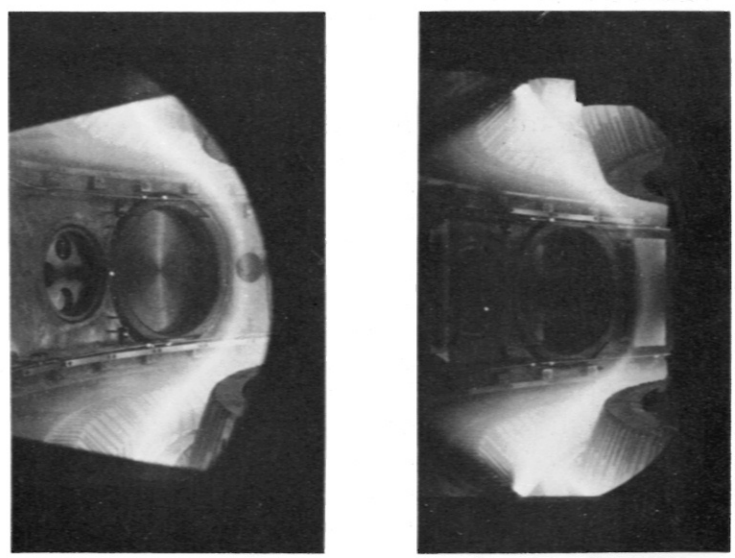

Fig.3
H_α-pictures of a divertor discharge (a) with and (b) without by-pass.

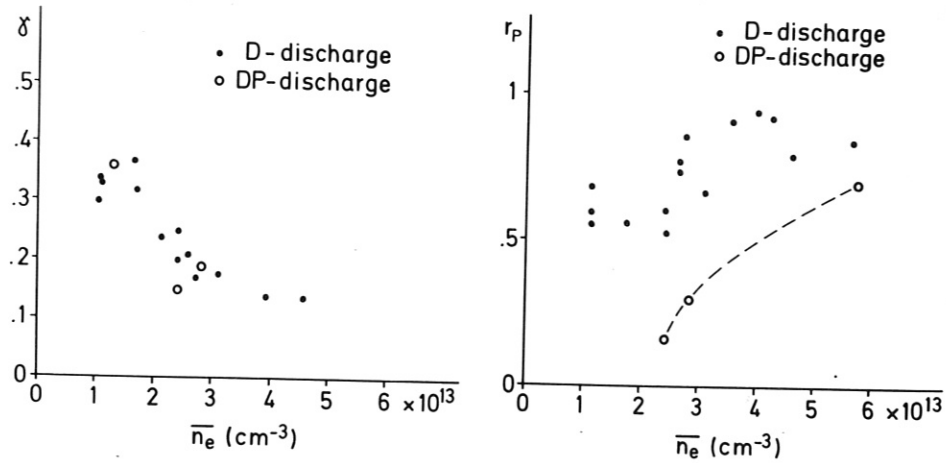

Fig.4
Fuelling efficiency γ and recycling coefficient r_p versus electron density $\bar{n}_e$.

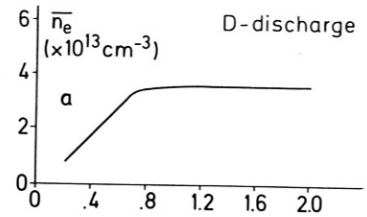

Fig.5
Time dependence of
(a) electron density $\bar{n}_e$,

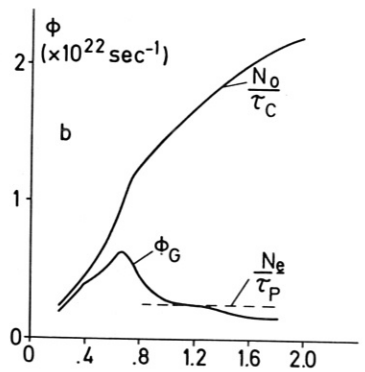

(b) external gas flux Φ_G, recycling flux N_o/τ_c and plasma loss flux N_e/τ_p,

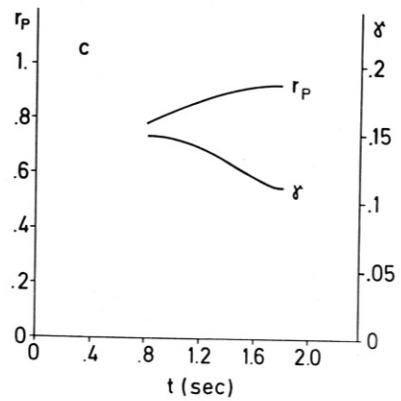

(c) recycling coefficient r_p and fuelling efficiency γ.

TOTAL RADIATION LOSSES IN THE OHMICALLY HEATED ASDEX TOKAMAK

The ASDEX Team
presented by E.R. Müller

Max-Planck-Institut für Plasmaphysik
EURATOM-Association, D-8046 Garching

One of the principle objectives of ASDEX is to demonstrate the high efficiency of an axisymmetric divertor in reducing the radiation losses in the core of the main plasma. The dissipation of the major part of the diverted power by isotropic emission of radiation and neutral particles in the divertor chambers /1/ is an experimental result which may have considerable implications in the design of larger tokamaks.

ASDEX discharges with ohmic heating can be classified according to L = limiter discharges, D = divertor discharges, DP = divertor discharges with Ti-gettering inside the divertor chambers. In order to compare the energy balance of different types of discharges, ASDEX offers the possibility of performing transitions between them during one series of shots with some of the plasma parameters fixed at constant values /2/. The result is shown in Fig. 1. The difference between the ohmic input power OH and the bolometrically measured radiation and particle losses in both the main plasma volume and the divertor chambers can be interpreted as convection losses to the surfaces of the limiter (L type) or the target plates (D or DP type).

Whereas the magnitude of the ohmic input power varies with alternating discharge type its centre peaked profile shape keeps the same (Fig.2 of Ref./3/). On the contrary, the corresponding total radiation profiles differ drastically (Fig. 2). In L discharges the stainless-steel limiter contaminates the plasma mainly with iron corresponding to a high radiation level of 65 - 85 % of OH. Comparison of the D and DL[+)] radiation profiles indicates that with increased plasma-limiter interaction the centre radiation losses grow by more than one order of magnitude. The D radiation profile (radiation RAD amounts to 33 % of the 300 kW input power) is characterized by nearly vanishing centre radiation and a peripheral radiation layer mainly due to oxygen VUV line radiation, but CX losses cannot be neglected. Additional Ti-gettering reduces the oxygen

---

[+)] In DL discharges the divertor multipole currents are switched on and the limiter is positioned at the separatrix in order to get discharges sufficiently reproducible for performing a bolometric scan measurement from shot to shot.

content of the plasma and, hence, the edge radiation emission. The consistency of the sources of the residual radiation amounting to 10 - 15 % of OH is unexplored as yet, probably a high portion of CX losses being included.

When the poloidal plasma asymmetry is systematically varied by vertical displacement of the plasma column the radiation and neutral particle losses in the two outer divertor chambers (upper out and lower out) scale linearly with the corresponding divertor electron line density $\int n_{eDIV} \cdot dl$ (Fig.3). On the assumption that the same scaling law is valid for the inner two divertor chambers (upper in and lower in), it is possible to determine the total radiation and neutral particle losses in all four chambers RAD_{DIV} by measuring them in one chamber but $\int n_{eDIV} \cdot dl$ in each of the four chambers (the diagnostic arrangement is shown in Fig. 1 of Ref. /4/). At $I_p = 250$ kA, $\bar{n}_e = 2.8 \times 10^{13}$ cm^{-3} about 1/2 of the energy flowing into the divertor is lost by bolometrically measured radiation and neutral particle emission. Fig. 3a indicates an exponential decay of divertor radiation as a function of Δz, the decay length amounting to 1.4 cm. Assumming uniform emission in a divertor radiation layer of this width one obtains a local emission of about 700 mW/cm^3.

From measurements with a LiF window in front of the bolometer it is concluded that Hα and Lα radiation contribute less than 10 % to RAD_{DIV}. VUV line radiation due to impurities cannot explain the order of magnitude of the observed power losses; this was confirmed by spectroscopic measurements in the divertor chamber. Neutral particle emission above 100 eV measured by a neutral particle analyzer shows no correlation with the bolometric signal. There are two strong arguments for neutral particles in the 10 eV range constituting the main energy loss channel: Firstly, during a D-DP transition the bolometric signal of the fourth DP shot is significantly lower than that of the last D shot at the beginning of the discharge; at the end of the discharge the DP signal approaches the D signal (Fig.4). This qualitative behaviour can only be observed in signals correlated with hydrogen such as the gas feed rate or the neutral gas pressure in the divertor. It is interpreted as the vanishing efficiency of a thin titanium layer in pumping the hydrogen. Secondly, resonant charge exchange (CX) is an atomic process which could explain the rather high energy losses: neutrals in the 1 eV range undergo resonant CX in a plasma layer with $n_i \approx 2 \times 10^{13} cm^{-3}$ and $T_i \approx 10$ eV within a distance of about 2 cm. 10 eV CX neutrals escaping from the plasma layer would provide energy losses of about 3 W/cm^3 if all the hydrogen within the layer is dissociated.

Figure 5 shows the variation of the divertor energy balance with $\int n_{eDIV} \cdot dl$ and I_p. The fraction of the divertor input power INP_{DIV} (assumed as OH-RAD) which is lost by radiation plus neutrals attains values of up to 70 % with increasing $\int n_{eDIV} \cdot dl$. This is mainly due to the fact that RAD_{DIV} scales approximately linearly with $\int n_{eDIV} \cdot dl$, which again has a nonlinear dependence on $\bar{n}_e$ (Fig.5 of Ref./3/). At $I_p = 400$ kA the ratio RAD_{DIV}/INP_{DIV} is slightly higher than at $I_p = 250$ kA for fixed $\int n_{eDIV} \cdot dl$, but also higher values of $\int n_{eDIV} \cdot dl$ can be realized at higher current.

Conclusions

- In L discharges the SS-limiter is the main impurity source and radiation consitutes the totally dominating energy loss channel.
- The divertor reduces the centre radiation losses due to impurities with a higher Z, dominantly iron; RAD/OH is decreased to between 32 % (250 kA-discharge) and 20 % (400 kA-discharge)
- In Ti-gettered divertor discharges (DP) the radiation losses are reduced to 12 %, an almost negligible residue in energy balance. One gets an extremely clean plasma characterized by $Z_{eff} = 1$.
- The ohmic heating power is normally deposited in the plasma centre. The energy losses of the core of D and DP plasmas are dominated by electron heat conduction.
- In high current ($I_p = 400$ kA) and high density ($\bar{n}_e = 6 \times 10^{13}$ cm^{-3}) discharges up to 55 % of the ohmic input or 70 % of the diverted power are dissipated in the divertor chambers by bolometrically detectable energy losses. RAD_{DIV} scales fairly linearly with $\int n_{eDIV} \cdot dl$.
- The main energy loss channel in the divertor is consituted by neutral particles in the 10 eV range presumably due to resonant CX.

References

/1/ Keilhacker,M. et al.: Proc.8th Int.Conf.on Plasma Physics and Contr. Nucl.Fus.Res., Brussels (1980), Vol. II,IAEA-CN-38-01
/2/ Niedermeyer,H. et al.: J.of Nucl.Mat. 93&94 (1980) 286
/3/ Keilhacker,M.: this conference, paper I.R3
/4/ Müller, E.R., Niedermeyer, H., IPP Report IPP III/74, Garching (1981)

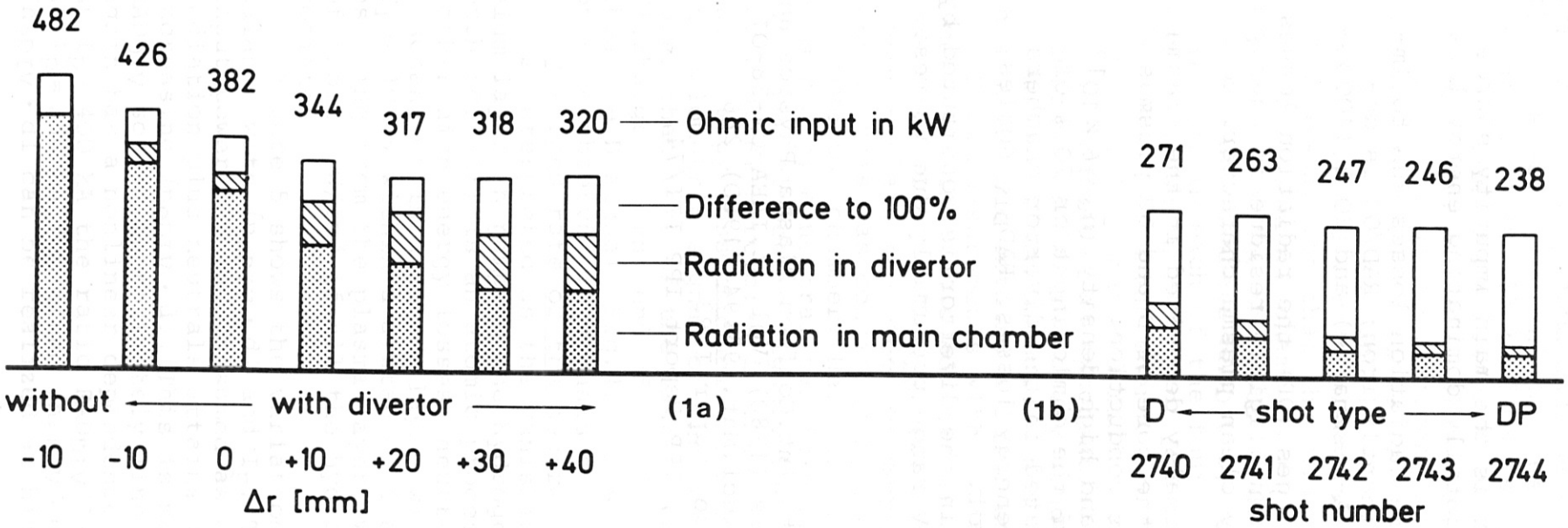

Fig.1: a) Energy balance for a transition from L to D discharges. A point limiter with a stainless steel tip was retracted from the plasma shot by shot, thus, increasing the radial distance Δr of the limiter to the separatrix. ($I_p = 275$ kA; $\bar{n}_e = 2.3 \times 10^{13} cm^{-3}$; $q_a = 3.9$).

Fig.1: b) Energy balance for a transition from D to DP discharges. Titanium was evaporated on the getter panels before every shot. The data are evaluated at 800 ms (see Fig.4). ($I_p = 250$ kA; $\bar{n}_e = 2.8 \times 10^{13} cm^{-3}$; $q_a = 4.3$).

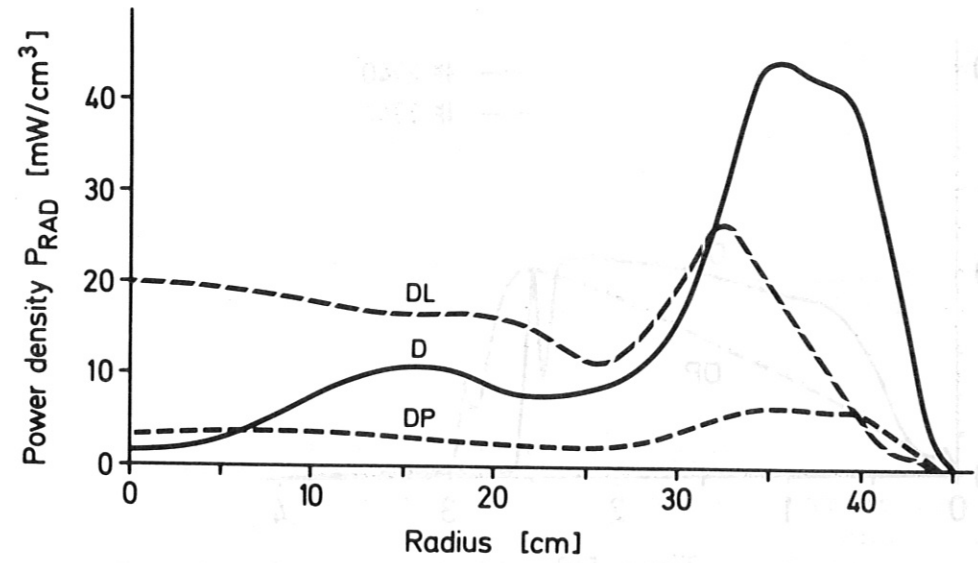

Fig.2:
Total radiation profiles of different types of discharges.
(I_p=250 kA
$\bar{n}_e$= 3.0×10^{13}cm^{-3}
in the case of DP:
$\bar{n}_e$=2.3×10^{13}cm^{-3}).

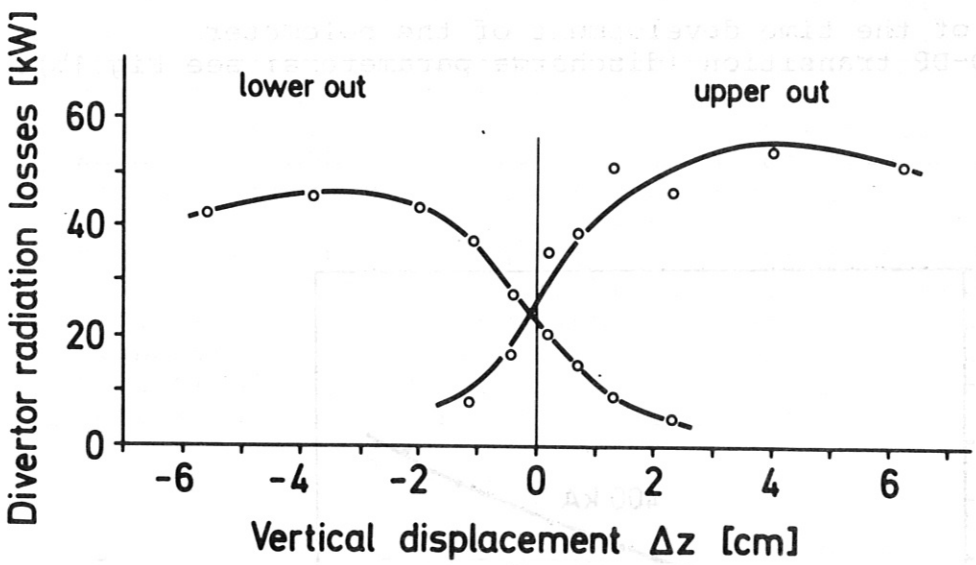

Fig.3:

a) Total radiation losses in the upper outer and lower outer divertor chamber vs. vertical displacement Δz of the plasma column
(I_p=250 kA
$\bar{n}_e$=2.0×10^{13}cm^{-3}
q_a=4.3).

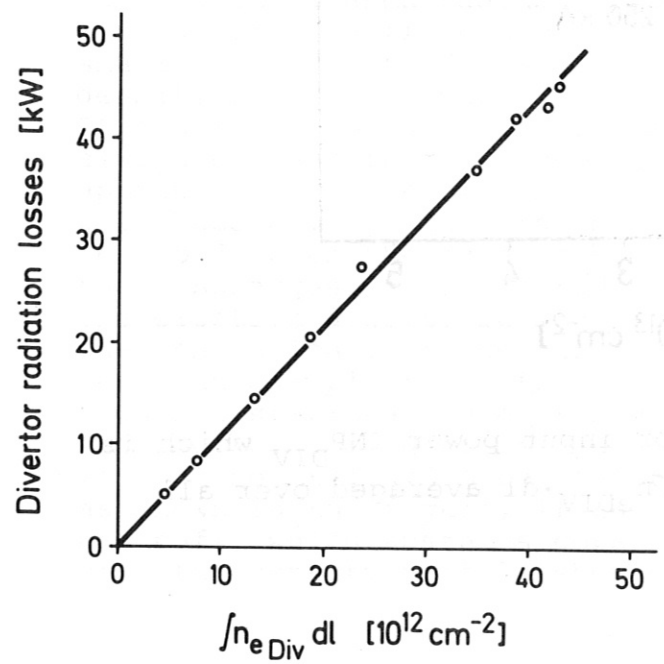

b) Scaling of the radiation losses in one chamber with the corresponding electron line density during vertical displacement of the plasma column.

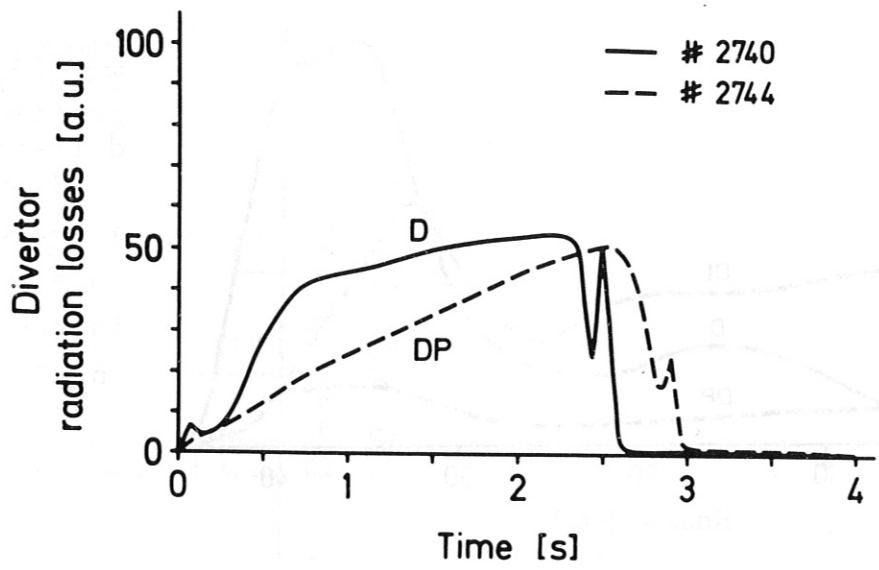

Fig.4: Variation of the time development of the bolometer signal during a D-DP transition (discharge parameters: see Fig.1b).

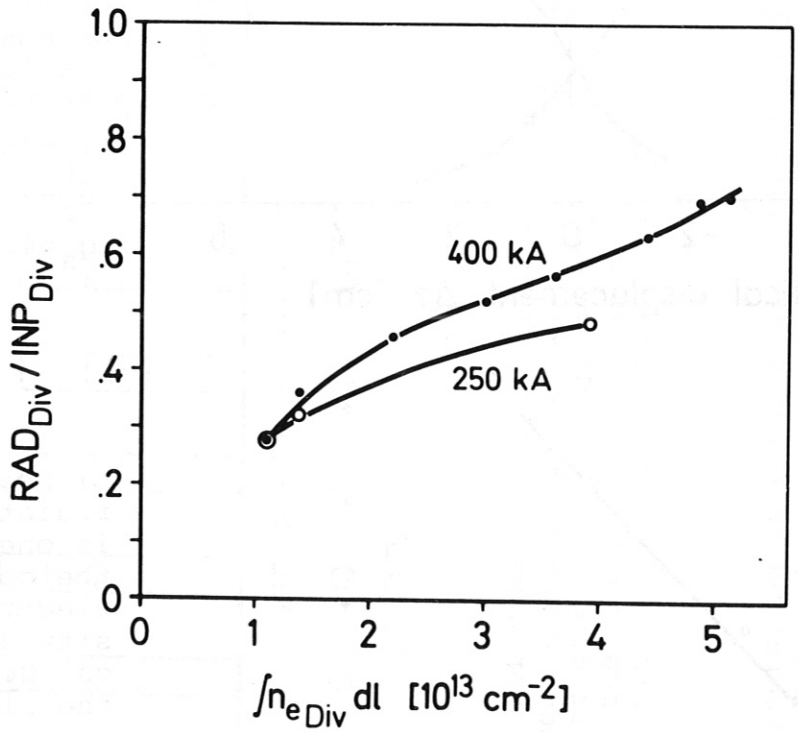

Fig.5: The fraction of the divertor input power INP_{DIV} which is lost via RAD_{DIV} is a function of $\int n_{eDIV} \cdot dl$ averaged over all four chambers.

PARTICLE TRANSPORT PHENOMENA IN ASDEX

K. Behringer, W. Engelhardt, G. Fussmann
and the ASDEX Team,

Max-Planck-Institut für Plasmaphysik
EURATOM-Association, D-8046 Garching

I. Transport within the separatrix

The transport of particles in tokamaks can be determined experimentally by measuring the sources and sinks as well as the spatial particle distribution, and by applying the continuity equation. In practice only a radial particle flux averaged over a magnetic surface can be obtained in this way. The determination of poloidal and toroidal fluxes demands much more precise information on the particle density distribution than it is available at present.

The radial flux of hydrogen in the centre of a large tokamak like ASDEX is very small. The corresponding particle confinement time is of the order of 3 s. On the other hand, impurities seem to diffuse at a much faster rate as may be concluded from the fact that they are not distributed according to corona ionization equilibrium. These observations could imply that hydrogen and impurity ions obey quite different transport laws. A unified description, however, of the transport of all kind of particles is obtained, if one uses the following expression for the mean radial flux:

$$\Gamma_k = -D \left(\frac{\partial nk}{\partial r} + \frac{2r}{a^2} n_k\right)$$

n_k is the density of particles of type k, a is the limiter (separatrix) radius, D is a diffusion coefficient which may depend on the plasma radius r. Without the (second) convective inward term, particle profiles are flat when the flux Γ_k is small. In order to describe the peaked nature of the electron density profiles, Coppi /1/ has introduced a similar expression. It should be noted, however, that the stationary profiles can always be described without an additional inward term by an appropriate choice of D(r). In large tokamaks the size of D will become very small in the center. This concept does no longer hold, when the dynamic behaviour of instationary phases of the discharges is considered. On Pulsator and ASDEX we studied the electron density build-up and decay. The results led us to the conclusion that the particle flux contains the above inward term. An example taken from ASDEX is given in Fig.1. The measured stationary electron density profiles (points from Thomson scattering around curve a) together with the known profile of neutral hydrogen lead to a diffusion coefficient D(r) as shown in the figure, if the inward term is omitted. When the gas puff, which sustains constant density in time, is switched off, the density profile should decay according curve b after

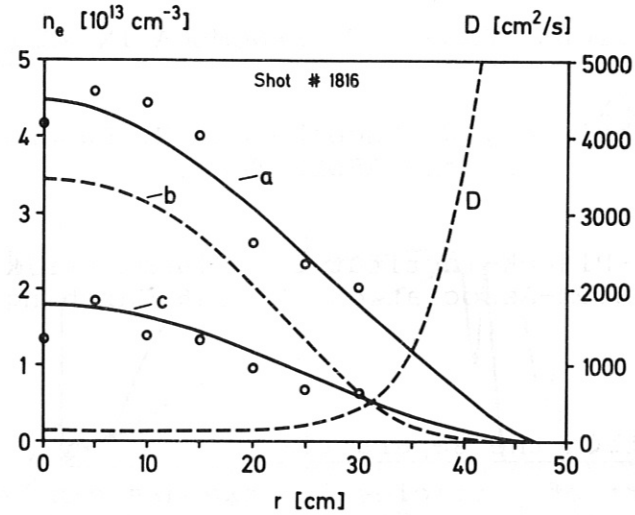

Fig. 1

O.6 s. This is not the case, but the density decays much faster (points around curve c). If the inward term is included, good agreement with the measured profiles is obtained both in the stationary (curve a) and the instationary case (curve b). The diffusion coefficient has to be chosen constant: D = 4000 cm^2/s.

The same diffusion coefficient can be used to describe the impurity profiles. A comparison of calculated and measured stationary oxygen profiles is given in Fig.2. The agreement is satisfactory. The existence of the inward term is consistent with the measured profiles, but it cannot be proven on this basis, because the impurity profiles have steep gradients such that the spreading term dominates the particle flux. By measuring the absolute ground state density of different ionization stages one could make a more reliable statement, but the necessary experimental accuracy is not available. It is obvious, however, that oxygen diffuses with a large diffusion coefficient in the plasma center, which would differ at least by an order of magnitude from D(r) (Fig.1) for hydrogen, if we were to omit the inward term.

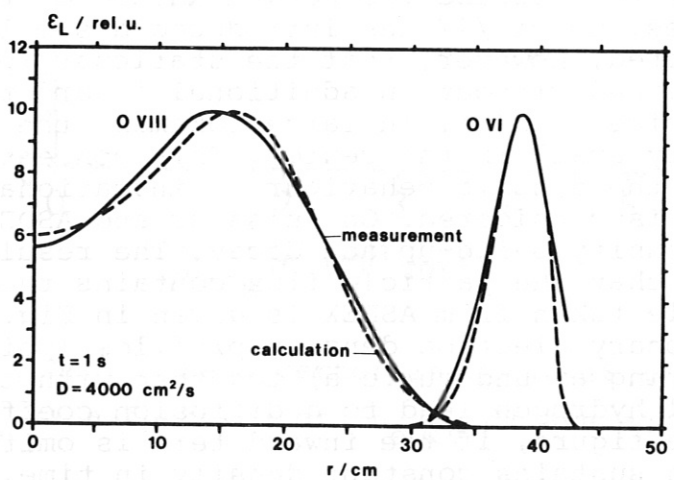

Fig. 2

An example for non-stationary impurity profiles is given in Fig.3. A Ne-puff of 5 ms duration was injected into a stationary hydrogen discharge and the development of the profiles was followed in time. The agreement between measurement (solid lines) and calculation 50 ms after the injection is again satisfactory. If D(r) from Fig.1 and no inward term is used to describe the profiles, it is found that the impurity ions do not penetrate fast enough into the plasma. For example, the Ne X shell (curve b, Fig.3) disagrees drastically with the measured profile in this case.

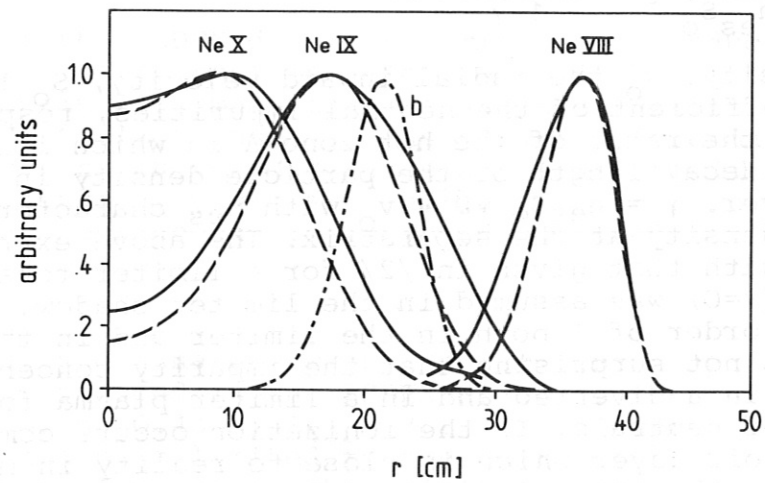

Fig. 3

The agreement between experiment and the simple transport model is obtained for sawtooth dominated discharges. During the start-up phase we observe accumulation phenomena which in rare cases persist during the whole discharge of 3 s. The sawtooth is then replaced by a large m=1 mode. Because of the rare occurrence of this phenomenon we have no systematic profile measurements, but it can be anticipated that our model would fail to describe these discharges. Poloidal asymmetries in the impurity profiles as well as in the hydrogen flux leaving the separatrix are observed. Our one dimensional model is not suited to describe deviations from cylindrical symmetry. A detailed investigation of these observations is under way. It may influence and improve our empirical transport model. Finally, it should be mentioned that the particular radial dependence of the inward term is based on measurements in the plasma center We have no experimental evidence that it also exists close to the plasma boundary. In the following section we have not included this term in our considerations.

II. Transport through the scrape-off layer

From measurements on low ionization stages of oxygen we find that a diffusion coefficient of 4000 cm^2/s holds also very close to the separatrix. It is then close to the Bohm--diffusion coefficient which may be accidental. If we assume that outside the separatrix in the scrape-off layer the trans-

port across the field is governed by the same diffusion coefficient, we can calculate the impurity content inside the separatrix for a given influx and known electron density and temperature profiles. In this case, the transport of particles parallel to the field into the divertor chamber has to be included. This is done roughly by using the concept of a confinement time $\tau_{\parallel} = L/v_{\parallel}$ where L is the length of a field line and $v_{\parallel}$ the flux velocity of the impurities parallel to the field. Solving the continuity equation we find for the sum(n_{tot}) over all ionization stages (excluding the neutral state) of an impurity inside the separatrix:

$$n_{tot} = \frac{n_o v_o^2}{D\, n_{es} S_o}\, e^{-\beta}\, \frac{e^{\beta(1-\gamma)} - \gamma^2}{1-\gamma}$$

n_o is the density, v_o the radial inward velocity, S_o the ionization coefficient of the neutral impurities, respectively. $\beta = \Delta/\sqrt{D\tau_{\parallel}}$ is the ratio of the hot zone Δ in which ionization occurs to the decay length of the particle density in the scrape-off layer. $\gamma = n_{es} S_o \sqrt{D\tau_{\parallel}}/v_o$ with n_{es} characterizing the electron density at the separatrix. The above expression is identical with that given in /2/ for a limiter tokamak, where $\tau_{\parallel} = 0$ ($\gamma=0$) was assumed in the limiter shadow. As β is always of the order of 1 both in the limiter and in the divertor case it is not surprising that the impurity concentrations differ little in a diverted and in a limiter plasma for a given influx of neutrals. If the ionization occurs completely in the scrape-off layer which is close to reality in many cases ($\gamma >> 1$), the total impurity density is independent of the electron density at the separatrix:

$$n_{tot} = n_o v_o e^{-\beta\sqrt{\frac{\tau_{\parallel}}{D}}}$$

The relative impurity concentration is then inversely proportional to the plasma density. These formulae have been satisfactorily verified by Ne injection experiments. They are also consistent with absolutely measured iron concentrations where the incoming flux was calculated by assuming that iron is sputtered at the wall by charge exchange neutrals.

The beneficial effect of the divertor on the impurity concentrations is apparently due to a reduction of the impurity influx which enters linearly in the expression for the impurity concentration. For oxygen the reduction of the source is due to the increased pumping speed by evaporating titanium in the divertor chamber. Iron is reduced, because the plasma-limiter contact is eliminated and the remaining sputtering processes at the torus wall constitute a much weaker source at least in the ASDEX plasma with moderate temperatures.

References

/1/ B.Coppi, N.Sharky, in "Physics of Plasmas close to Thermonuclear Conditions", Proc. of a course held in Varenna, 1979, EUR FU BUR/XI/476/80

/2/ W.Engelhardt, W.Feneberg, J.Nucl.Mat. 76&77 (1978) 518

LONG PULSE SUPRATHERMAL DISCHARGES IN THE ASDEX TOKAMAK +)

G.Fußmann,D.Campbell,A.Eberhagen,W.Engelhardt,F.Karger,
M.Keilhacker,O.Klüber,K.Lackner,S.Sesnic,F.Wagner,
and the ASDEX-team

Max-Planck-Institut für Plasmaphysik
EURATOM-Association, D-8046 Garching

Abstract:

Use of the ASDEX divertor permits the production of stable low density discharges ($n_e \gtrsim 10^{12}cm^{-3}$) with extremely low resistivity lasting for more than 10 seconds. While the distribution functions of electrons and ions show suprathermal tails, runaway electrons in the MeV range are found to disappear with decreasing density. There are indications that in these discharges the energy confinement is improved compared to scaling laws generally invoked.

Recently discharges with a pulse length up to 12 seconds have been produced in the ASDEX divertor tokamak (Ref. /1/, $R_o = 1.65$ m, $a = 0.40$ m, $B_{tor} = 2.2$ T). In normal discharges the pulse duration is limited to approximately 3 s by the available transformer flux swing. This limitation is overcome in clean, extremely low density discharges where increased plasma conductivity leads to a reduction of the loop voltage by an order of magnitude. The divertor is found to play an important role in these experiments: it prevents plasma pollution and enables very low density operation by reducing the recycling from the walls. In these discharges limitations in the toroidal field power supply determine the discharge duration.

In Fig.1 the time dependence of six essential parameters for a typical long pulse discharge is shown. For the time interval 0.6 - 0.78 s a density plateau of $\bar{n}_e = 2.5 \times 10^{13}cm^{-3}$ is set by feedback control. Thereafter the hydrogen gas inlet valve is closed. The density then decays to $5 \times 10^{12}cm^{-3}$ within 100 ms and reaches a lower limit of $1 - 2 \times 10^{12}cm^{-3}$ after a few seconds. This asymptotic limit is probably sustained by hydrogen outgassing from the walls. Also shown in Fig.1 are the traces of the electron temperature according to electron cyclotron emission (ECE, 2nd harmonic), the plasma current (~250 kA), the loop voltage (U_L, falling from 1.2 V to 0.12 V), the soft X-ray intensity emitted by the plasma(70 eV < hν < 30 keV) and the hard X-rays released by impact of runaway electrons at a stainless steel limiter 7 cm beyond the magnetic separatrix at the outer side of the torus.

+) An extended version of the paper has been puplished in Phys.Rev.Lett. 47, 1981, 1004

Thomson scattering, soft X-ray pulse height analysis (PHA) and ECE-measurements yield equal electron temperatures of 0.7 keV during the density plateau from 0.6 - 0.78 s in Fig.1. Thereafter Thomson scattering fails because the density is too low, but the ECE indicates - in agreement with PHA measurements - a rapid increase in T_e to 1.5 - 1.6 keV at 0.96 s. At this time an electron energy confinement time of about 25 ms is obtained. After that time the development of a weak suprathermal tail in the electron distribution function is inferred from soft X-ray PHA-measurements. This is also indicated by a steep increase in the ECE (dotted part of T_e in Fig.1) to intensities which, for a thermal and optically thick plasma, would correspond to electron temperatures above 1o keV at 1.2 s. From the slope of the PHA-spectra (available only for $t \leq 1.4$ s) an electron temperature of approximately 2.o keV and a corresponding confinement time of 5o ms are obtained at $t = 1.4$ s.

In contrast to what is generally expected, the hard X-ray flux from the limiter is seen in Fig.1 to decrease with decreasing density and to disappear almost completely after a few seconds. Furthermore, for discharge durations $\gtrsim 5$ s no final burst of hard X-rays is observed, neither from the limiter nor from other parts of the torus. Whereas the initial rapid decrease of the hard X-ray signal is probably enhanced by an inward shift of the runaway drift-surfaces resulting from a decrease in pressure (β_{pol}) and a peaking of the current profile, a deceleration of the runaways must also be assumed to explain these observations. The minimum value of their original kinetic energy is known to be 1o MeV. Since the transparency of the torus vessel is greater than 1o % for photon energies above 3oo keV, the decrease in the hard X-ray signal implies that the runaways are slowed down from 1o MeV to less than a few hundred keV. Such deceleration cannot be attributed to Coulomb friction, as is demonstrated by calculating the slowing down time for the relativistic electrons: even neglecting the accelerating electric field it amounts to 7.5 s for 1o MeV particles at $n_e = 5 \times 1o^{12} cm^{-3}$ /2/. Moreover, it is observed that the electron density decays more rapidly than the loop voltage. Hence, the accelerating field decreases more slowly than the Coulomb drag force and no slowing down is to be expected. For this reason an additional loss mechanism such as particle-wave interaction must be postulated to explain the observed deceleration. While the theory of beam wave-interactions suggests that the deceleration of non-relativistic runaways may take the form of the Cherenkov effect /3/, for relativistic electrons cyclotron radiation losses following particle pitch angle scattering by these waves might be more effective.

During the stationary low density phase ($t > 2$ s) of the discharge the total power input is only 3o kW. According to bolometer measurements the radiation losses amount to a few kW. If, for this period, the suprathermal character of the discharge is neglected an electron temperature of $T_{eo} = 3.7$ keV may be deduced from Spitzer conductivity assuming no temporal variations in the effective charge number $\bar{Z}$ and in the shape of the temperature profile. Furthermore, with the reasonable assumption of a parabolic profile for n_e and a squared para-

bola for T_e, an electron energy confinement time of 12o ms - which is larger than the maximum confinement time of 6o ms at high densities - is inferred. Note, however, that in these considerations the relation between conductivity and electron energy content for a thermal plasma is implicit and for a suprathermal discharge this may lead to an overestimation of the confinement time, since in such a case a larger fraction of the current can be carried by a beamlike tail of the distribution function. To obtain a criterion for the suprathermal contribution to conductivity we determine the runaway parameters E/E_D, i.e. the ratio of the induced electric field to the Dreicer field. In addition an estimate on $\bar{Z}$ is obtained by assuming $q(o) = 1$, where $q(r)$ is the safety factor. Combining the latter condition - which for $t \lesssim 0.8$ s could be substantiated by the observation of soft X-ray saw-tooth activity - with Spitzer's conductivitiy, we obtain at $t = 0.8$ s by comparison with measured temperatures $\bar{Z} = 1.4$ and $E/E_D = 0.006$. At $t = 0.96$ s, $\bar{Z}$ is found to have increased to 1.7 and E/E_D has reached its maximum of 0.03 ± 0.01. According to theory /4/, however, there should still be only a marginal suprathermal enhancement of the conductivity ($\lesssim$ 1o %) for this value of the runaway parameter. Furthermore, the runaway production rate /5/, which increases exponentially with E/E_D, is very small: $\dot{n}_{run}/n_e \sim 5 \times 10^{-3} s^{-1}$ at $t = 0.9$ s.

Apart from the technological achievement - tokamak discharges with a duration of 12 s have been obtained without difficulty - there are a number of physical aspects of these low density discharges which are of interest. In particular, we have found indications that the energy confinement is much better than predicted by ALCATOR-scaling ($\tau_E \propto n_e a^2$) which, for the lowest densities, yields $\tau_E \sim 2$ ms. Although we cannot completely exclude the possiblity of a cold electron bulk with temperatures much less than 1 keV, in general our findings are consistent with a bulk temperature of approximately 1.5 keV. These electron temperature and the very low power input result in an electron energy confinement time of the order of 5o ms. Furthermore, additional heating or current drive studies by RF or neutral injection appear rather attractive in this regime in view of the small number of particles.

References:

/1/ Keilhacker,M. et al., "Impurity Control Experiments in the ASDEX Divertor Tokamak", Proc. 8th Int.Conf.on Contr.Nucl. Fus.Res., Brussels 198o, Vol.II, IAEA-CN-38-O1, 351
/2/ Fußmann,G., Nucl.Fus. 19 (1979), 327-334
/3/ Parail,V.V. and Pogutse,O.O., Nucl.Fus.18 (1975) 3o3-314
/4/ Kulsrud,R.M., Sun,Y.C.,Winsor,N.K. and Fallon,H.A., Phys. Ref.Let. 31 (1973) 69o-693
/5/ Connor,J.W. and Hastie,R.J., Nucl.Fus.15 (1975) 414-424

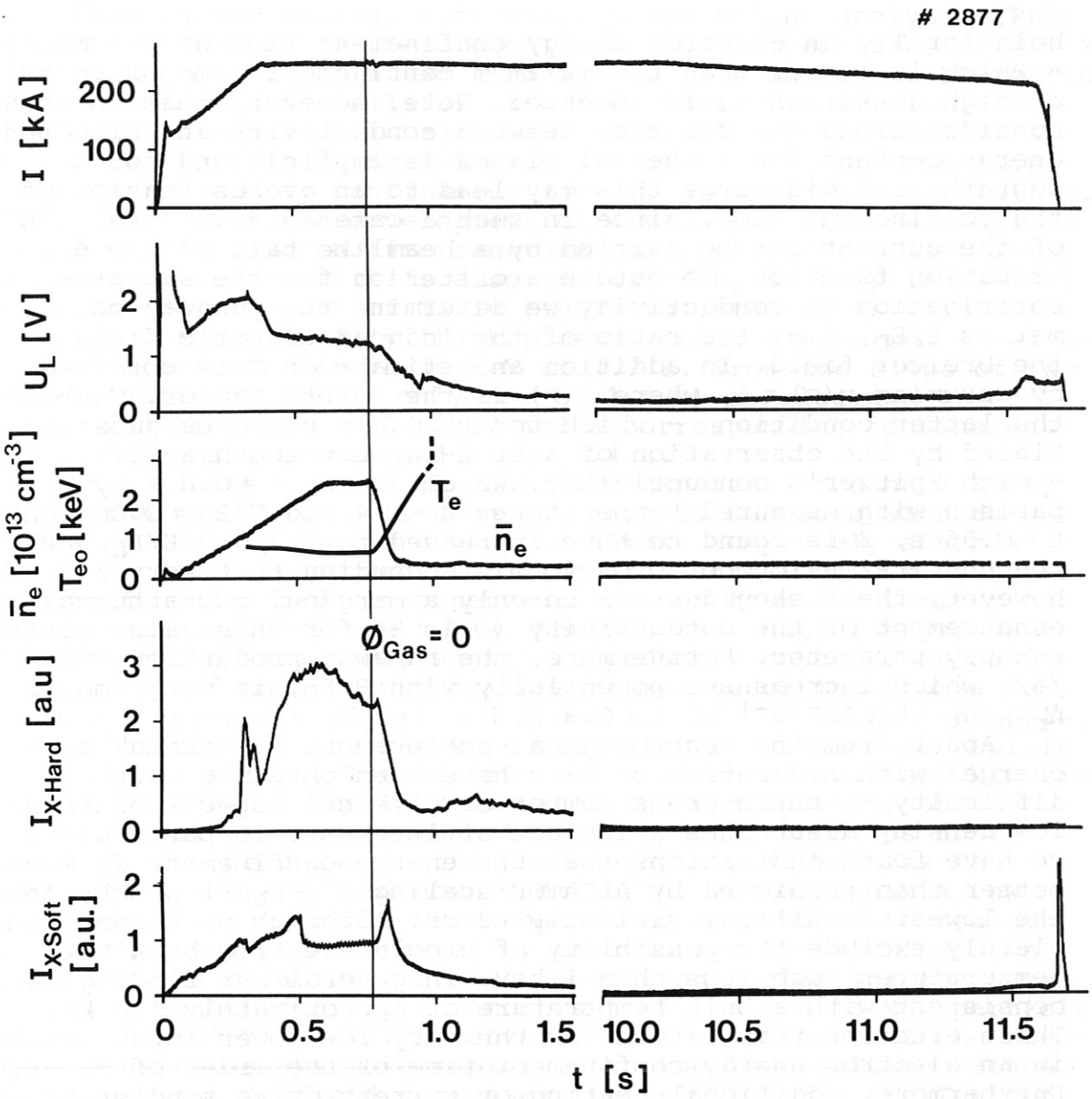

Fig.1: Time dependence of various plasma parameters in a long pulse discharge (notice the break of time scale).

MEASUREMENT OF THE DENSITY AND MEAN VELOCITY OF TITANIUM ATOMS IN FRONT OF THE ASDEX DIVERTOR PLATES BY LASER INDUCED FLUORESCENCE

E. Dullni, Sonderforschungsbereich "Plasmaphysik Bochum-Jülich", Ruhr-Univ. Bochum
P. Bogen, E. Hintz, D. Rusbüldt, B. Schweer, Institut für Plasmaphysik der KFA-Jülich GmbH, Association EURATOM-KFA
S. Goto[+], K.H. Steuer, Max-Planck-Institut für Plasmaphysik, Association EURATOM

ABSTRACT Density ($3 \times 10^{7} - 2 \times 10^{8}$ cm^{-3}) and mean velocity (3×10^{5} cms^{-1}) of Ti-atoms in front of the ASDEX divertor plates have been measured by means of laser induced fluorescence. The ambient electron density - measured by an interferometer - varied between $10^{12} - 10^{13}$ cm^{-3} and the electron temperature derived from the measured ionization length was around 10 eV. The flux of Ti-atoms is calculated. There is clear evidence that it is caused by hydrogen sputtering.

I. INTRODUCTION The target plates of the divertor are the principle regions of contact between the plasma and the wall of divertor tokamaks. As a result of this contact Ti-atoms are released and expand into the divertor chamber with a mean velocity $\bar{v}_{Ti}$ which is determined by the release mechanism. Depending on the electron density n_e and the electron temperature T_e of the divertor plasma particles get ionized and subsequently their orbits are determined by the local forces. It is obvious that for an understanding of divertor action the knowledge of the density, the flux density and the velocity distribution of the impurity atoms (and of the ions) is needed. Moreover, the measurement of these quantities may offer an excellent possibility to study processes of plasma surface interaction under realistic, however, comparatively well defined conditions.
A suitable diagnostic method which produces negligible perturbation of the plasma and which offers high sensitivity and excellent space and time resolution is the laser induced fluorescence of the impurity atoms. It is described briefly in / 1/. The detection limit of the method can be as low as 10^{5} particles/cm^{3}, the velocity resolution is of the order 5×10^{4} cm/sec.

II. EXPERIMENTAL ARRANGEMENT Most of the measurements reported here were done in the DP mode of the ASDEX experiment /2/ at B_T = 2 T, I_p = 300 kA, τ_{FT} = 3 s and with a plasma of: $n_e = 1 - 4 \times 10^{13}$/cm^{3}, T_e = 1 KeV, T_i = 500 eV; Z_{eff} = 1.
The density of Ti-atoms n_{Ti} in the divertor chamber was measured as shown in Fig. 1. Fig. 2 shows the relevant energy levels of Ti. The laser was tuned to the resonance transition at 294.2 nm. The fluorescence light which electrons emit when they decay into the b^3F metastable level is detected. At high laser power the integral of the fluorescence light corrected by a calibration factor yields directly the density of groundstate atoms $n_{Ti,0}$. The dye-laser after frequency doubling provides 800 W for about 0.5 μs.

III. RESULTS The fluorescence signal is calibrated by the Ti-vapor density when the evaporation pumps are active. From the measured amount of sublimated material one obtains at the point of observation a density of 1×10^{9} cm^{-3} (Fig. 3 a). Fig. 3 b shows

[+]on leave from Osaka University

for comparison a fluorescence signal taken during a plasma discharge. For the conversion of the fluorescence signal - which is proportional to $n_{Ti,0}$ - into the total density n_{Ti} one has to take into account the relative population of the fine-structure levels of the atoms emitted by the divertor plates, which may be different from that of the evaporated atoms. Thus, the average density of neutral titanium in the scattering volume is deduced to be 1.7×10^8 cm^{-3} with an error of about a factor of two.

In order to learn whether the Ti-atoms were evaporated or sputtered we need the approximate value of $\bar{v}_{Ti}$. Considering that the Doppler broadened absorption profile of the Ti-line is cut off at λ_o = 294.196 nm since negative velocities do not exist and will not extend beyond energies exceeding the cut-off value for ion sputtering (o.1 of the proton energy) it appears that an approximate value of v_{Ti} can be obtained by scanning with the 7 pm wide laser line across the Ti-line (FWHM $\approx$ 4 pm). One expects a profile the center of which is shifted to the red by about $\Delta\lambda = \frac{\lambda_o}{c} \bar{v}_{Ti}$. Fig. 5 a shows the absorption profile taken during the sublimation period. It corresponds to the laser profile because of the small velocity spread of evaporated atoms. The profile in Fig. 5 b exhibits a more complicated structure: As the laser light is reflected at the neutralizer plates, the atoms will be at resonance too, with the laser tuned to the blue. Thus the profile consists of two symmetric peaks the relative heights of which are determined by the reflection coefficient of titanium (25 %) and the degree of saturation of the fluorescence light. From the distance between the two peaks $\bar{v}_{Ti}$ is obtained $\bar{v}_{Ti} = 3 \times 10^5$ cm/s , which is in the same range as those velocities measured for Ti- or Fe-atoms in ion beam sputtering experiments /1/, /3/. The mean energy of 2.2 eV is in any case large compared to that of evaporated atoms. The conjecture that the Ti-atoms arise from sputtering is supported by further measurements. When the filling gas is changed from hydrogen to deuterium the fluorescence light signal increases by a factor of 2.5 - 3 (Fig. 3c), the plasma conditions remaining nearly the same. The same factor is predicted for ions having a maxwellian energy distribution with KT_i = 1oo eV /4/.

T_e and n_e (Fig. 4) in front of the neutralizer plates are sufficiently high for ionization of the Ti-atoms by electron impact to become significant. The effect is described by :

$$l = \bar{v}_{Ti}/n_e\, S(T_e); \quad n_{Ti}(x) = n_{Ti}\,(0) \exp(-x/l) \qquad (1)$$

where l is the ionization length, $S(T_e)$ the ionization rate coefficient. Taking for example $\bar{v}_{Ti} = 3 \times 10^5$ cm/s, $n_e = 5 \times 10^{12}$ cm^{-3} and T_e = 5 eV, 2o eV and using values for S given by /5/ one obtains for l values of 13 mm and 3 mm resp. With the length of the observation volume l_o being 15 mm we may assume that for a wide rang of densities $l/l_o \ll 1$. In this case the fraction of Ti-atoms within l_o which is not ionized is $l/l_o \sim n_e^{-1}$. The flux of sputtered Ti-atoms is proportional to the flux of hydrogen ions to the neutralizer plate i.e. $\sim n_e$. Taking into account ionization the number of Ti-atoms in the observation volume therefore becomes independent of n_e. Accordingly above a certain electron density the fluorescence intensity should not increase with n_e. This behaviour is indeed observed in Fig. 4. To confirm the assumptions about the ionization length l experimentally, the experimental arrangement had to be changed in such a way that a space resolution of o.2 cm could be achieved. The measured $n_{Ti}(x)$ is shown in Fig. 6. From the ionization length l = 4.3 mm and $n_e = 5 \times 10^{12}$ cm^{-3} (at o.5 s), we derive from Eq. (1) an electron temperature of 1o eV. After correcting for ionization losses we obtain $n_{Ti}\,(0) = 6 \times 10^8$/cm^3 and $\Phi_{Ti} = \bar{v}_{Ti} \times n_{Ti}\,(0) = 1.8 \times 10^{14}$ atoms/cm^{2}s.

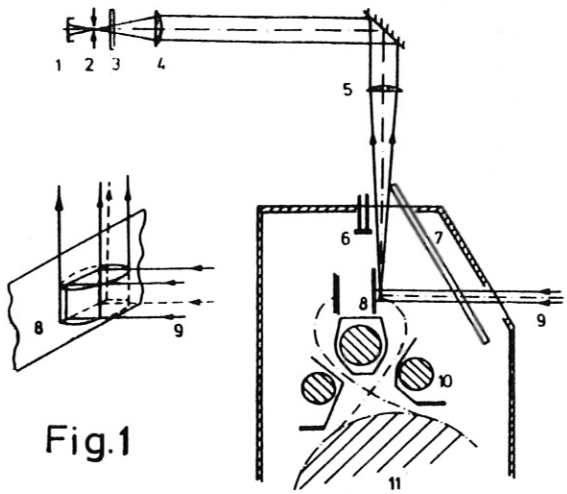

Fig.1

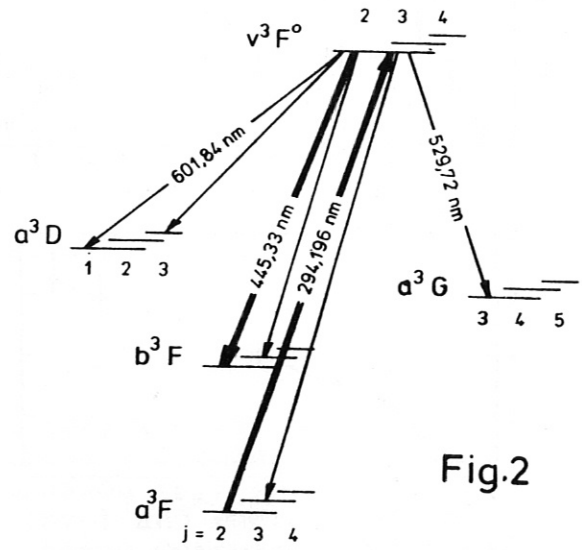

Fig.2

Fig. 1: Experimental arrangement with cross-section of ASDEX (1) photomultiplier, (2) diaphragm, (3) interference filter, (4) lens (f = 2o cm), (5) lens (f = 1oo cm), (6) film thickness monitor, (7) titanium evaporator, (8) neutralizer plates, (9) laser beam, (1o) multipole coils, (11) plasma

Figure 2: Energy levels of neutral titanium

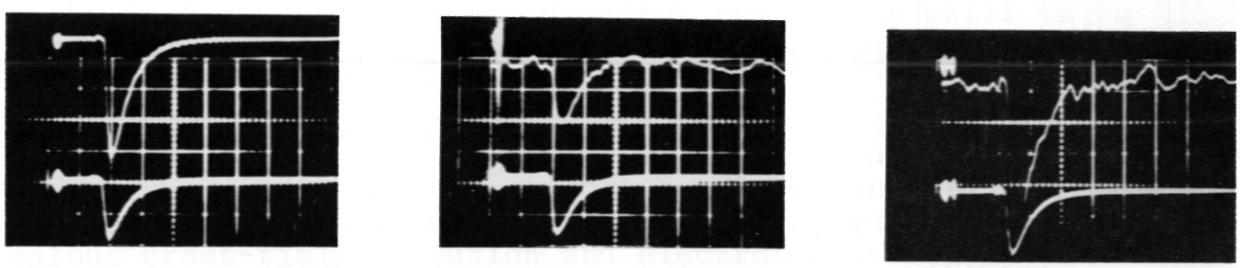

Fig. 3: Fluorescence light signals in front of the divertor plates (upper traces) and laser monitor (lower traces). a) Titanium evaporation, 1o mV/div, n = 1 x $1o^9$ cm^{-3}, b) discharge in H_2, 2 mV/div, c) discharge in D_2, 2 mV/div. Time scale 1 /us.

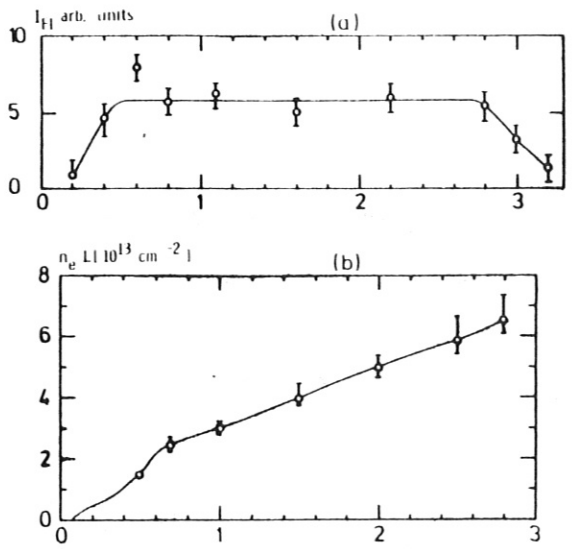

Fig. 4: Time dependence of the fluorescence signal and the electron line density n_e measured by a microwave interferometer. The distance L is about 5 cm.

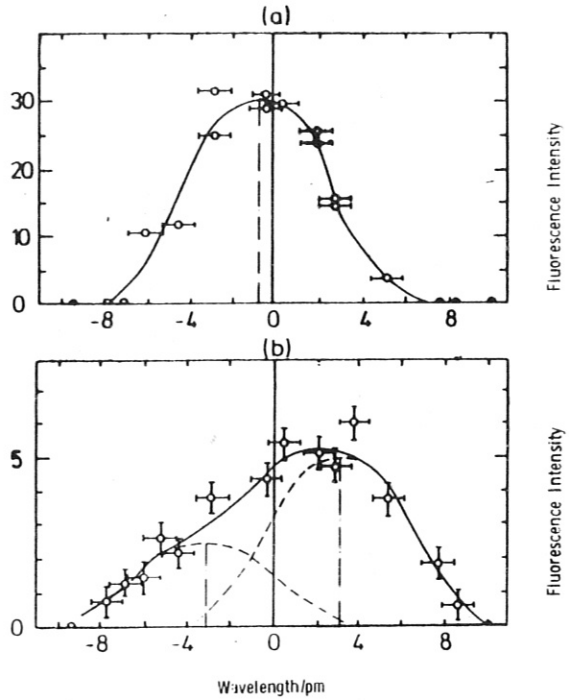

Fig. 5: Laser absorption profile of titanium atoms produced a) by evaporation, b) by the Tokamak discharge in hydrogen

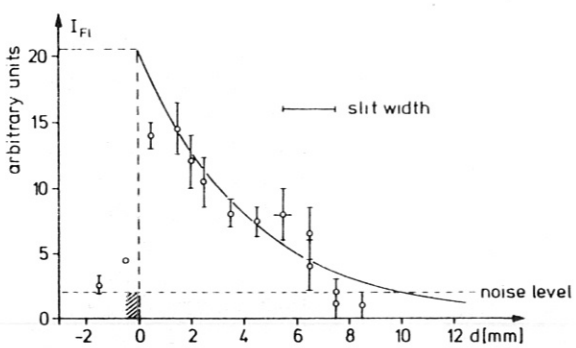

Fig. 6 Fluorescence signal of Ti atoms in front of the target plate as function of the distance from the plate.

REFERENCES

/1/ E. Hintz, J. Nucl. Mat 93/94 (1980) 86
/2/ M. Keilhacker, Divertor Experiments in ASDEX (this conference)
/3/ E. Dullni, E. Hintz, Verhandl. DPG (VI) 16, P 89 (1981)
/4/ J. Roth et al., IPP-Report No. 9/26, May 1979
/5/ W. Lotz, IPP-Report No 1/76 (1968)

SIMULATION OF THE SCRAPE-OFF REGION IN ASDEX

G. Becker, C.E. Singer[+)]

Max-Planck-Institut für Plasmaphysik
EURATOM-Association, D-8046 Garching

[+)] Princeton Plasma Physics Laboratory

Abstract:

Ohmically heated ASDEX discharges (DP, $q = 4.4$) are simulated by the BALDUR transport code with a 1-d scrape-off model. It includes anomalous cross-field diffusion ($D_\perp$) and electron heat conduction, convective particle (nv_Γ) and energy losses $\parallel \vec{B}$ and parallel electron heat conduction. Computed scrape-off lengths for n agree with $\lambda_n = (D_\perp \frac{\tau_i \cdot \tau_\parallel}{\tau_i - \tau_\parallel})^{1/2}$ and are independent of the recycling coefficient ρ. For $v_\Gamma = 0.1\ v_s$ and $D_\perp = 1.6 \cdot 10^3\ cm^2 s^{-1}$ ($\lambda_n = 1.5$ cm) one obtains $\rho = 0.2$. About 80 % of the scrape-off energy losses are due to parallel heat conduction and only about 20 % due to convection $\parallel \vec{B}$.

Introduction

The development of transport codes including the boundary of tokamaks is important for the understanding of the processes in the scrape-off region and for designing advanced tokamak devices. An attempt is made to take into account the essential physics in the edge region and to test the models against experimental results from ohmically heated divertor discharges in ASDEX. One difficulty is that the accuracy of many measurements in the scrape-off and divertor region has still to be increased in order to allow a clear distinction between different model assumptions.

Modeling and Code

The new version of the BALDUR transport code /1,2/ incorporates a self-consistent 1-d scrape-off region model with anomalous cross-field diffusion and electron heat conduction. Convective particle (nv_Γ) and energy losses $\parallel \vec{B}$ are simulated with a subsonic flow velocity, since the scrape-off zone of ASDEX is collision dominated. From experimental findings $v_\Gamma \approx 0.1\ v_s$ with the local sound speed $v_s = \left[\frac{2(kT_e + kT_i)}{m_i}\right]^{1/2}$ is derived and has been inputted in the computations. The energy delivered to the divertor plates and to the divertor plasma by the electrons and ions is $2\gamma_e kT_e$ and $2\ kT_i$, respectively. Secondary electron emission may be neglected ($\gamma_e = 2.9$) because the magnetic field lines graze the divertor plates and therefore force the secondary electrons back. In addition, losses due to electron heat conduction $\parallel \vec{B}$ ($\vec{q}_\parallel = -\kappa_e \vec{\nabla}_\parallel (kT_e)$) have been included. With a classical κ_e and $\mathrm{div}\ \vec{q}_\parallel = 0$ a $q_\parallel(r) \sim T_e(r)^{7/2}$ results that

limits T_e in the scrape-off zone due to its strong temperature dependence.

Moreover, a new fast "vectorized" version of the AURORA Monte-Carlo neutral transport coding has been implemented. Further improvements include feedback control of gas puffing for density programming and a wide variety of transport models to allow flexibility in fitting experimental data.

Results

Ohmically heated low density $q = 4.4$ ($B_t = 22$ kG, $I_p = 246$ kA) ASDEX discharges of type DP (divertor with pumping) are simulated with bremsstrahlung ($Z_{eff} = 1.2$). Line radiation from impurities is neglected because of the very low impurity level. In agreement with analytic steady-state solutions for the scrape-off region /2/ n, T_e, T_i and the flux decay $\sim\exp(-\frac{r-a}{\lambda})$, where a is the separatrix radius (4o cm) and λ is the corresponding scrape-off length. Variation of the cross-field diffusion coefficient $D_\perp$ (see Fig.1) shows that the density scrape-off length is in good agreement with $\lambda_n = (D_\perp \frac{\tau_i \cdot \tau_\parallel}{\tau_i - \tau_\parallel})^{1/2}$, where $\tau_i = (n_o \langle \sigma_i v_e \rangle)^{-1}$ and $\tau_\parallel = \frac{L}{v_\Gamma}$ is the average lifetime of a particle in the scrape-off zone. The result that λ_n is independent of the recycling coefficient ρ explains the agreement with the analytic relation that neglects recycling. In Fig.1 $\lambda_n = (D_\perp \tau_\parallel)^{1/2}$, which does not include ionization ($\tau_i \to \infty$), is also given for comparison.

Computed profiles for the above mentioned DP-discharges (see Fig.2a) are compared with the experiment in Figs.2b and 2c. For $v_\Gamma = 0.1\ v_s$ and $D_\perp = 1.6 \cdot 1o^3 cm^2 s^{-1}$ ($\lambda_n = 1.5$ cm) a best fit to the $\bar{n}_e$-decay after closing the gaspuff valve (see Fig.2a) is obtained with $\rho = 0.2$.

At $t = 1$ s the total ohmic heating power is 3o6 kW while the losses from neutral hydrogen and bremsstrahlung amount to 38 kW and 1o kW, respectively. Heat conduction and convection $\perp \vec{B}$ to the walls are negligible. The residual heating power equals the scrape-off losses due to heat conduction $\parallel \vec{B}$ (≈8o %; 2o4 kW) and due to convection (≈2o %; 54 kW). Thus, the dominant cooling mechanism in the scrape-off zone is parallel electron heat conduction. The strong limiting influence of $q_\parallel$ on $T_e(r)$ is demonstrated in Fig.3 (solid curve). Obviously, the model that includes convective losses alone (dashed curve) disagrees with T_e-measurements from laser light scattering. The total energy confinement time is found to be 47 ms.

In Fig.4 the essentially linear increase of λ_{T_e} with $\chi_{e\perp}$ is shown. It can be seen that a rather short scrape-off length of 0.4 cm results for $\chi_{e\perp} = 0$ which is caused by parallel electron heat conduction. The $\chi_{e\perp}$-value corresponding to $\lambda_{T_e} = 1.13$ cm as shown in Fig.3 amounts to $2 \cdot 1o^4 cm^2 s^{-1}$. Since the time of equipartition is only 0.3 ms, a rather close coupling between λ_{T_i} and λ_{T_e} results.

Gas puff neutrals and recycled neutrals are launched with 3.3 eV (Franck-Condon atoms). The computed gas puff rate of $1.8 \cdot 1o^{21}$ atoms s^{-1} at $t = 1$ s is consistent with the experiment.

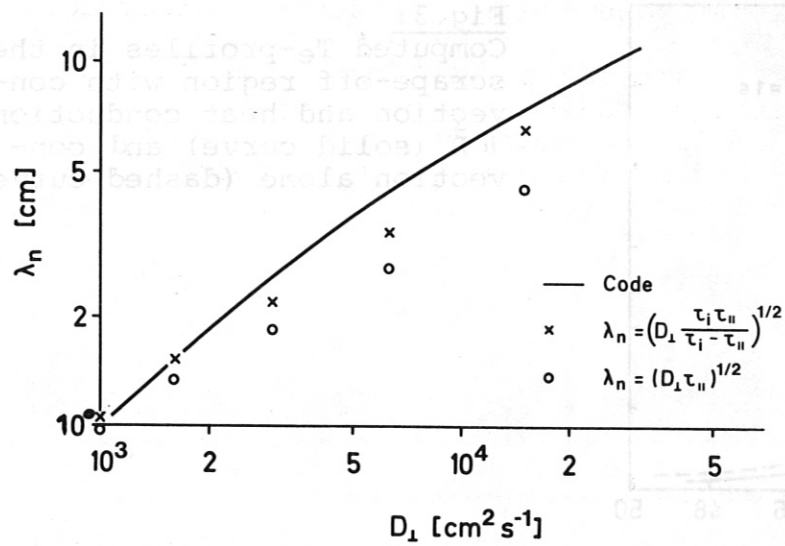

Fig.1:
Density scrape-off length λ_n vs. $D_\perp$ compared with analytic relations.

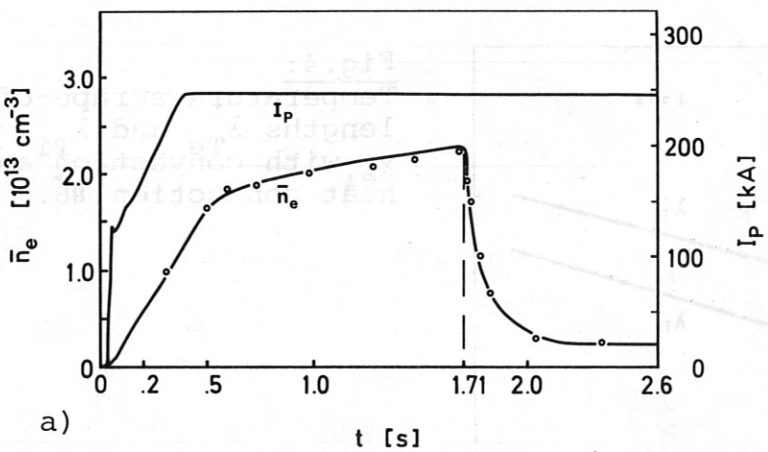

Fig.2:
Simulated ASDEX DP-discharges (q=4.4).
a) Programs of I_p and line averaged density $\bar{n}_e$ in experiment (solid curves) and computation (circles).
b) and c) Experimental (circles) and code results (solid curves) for t=0.5 and 1.0 s.

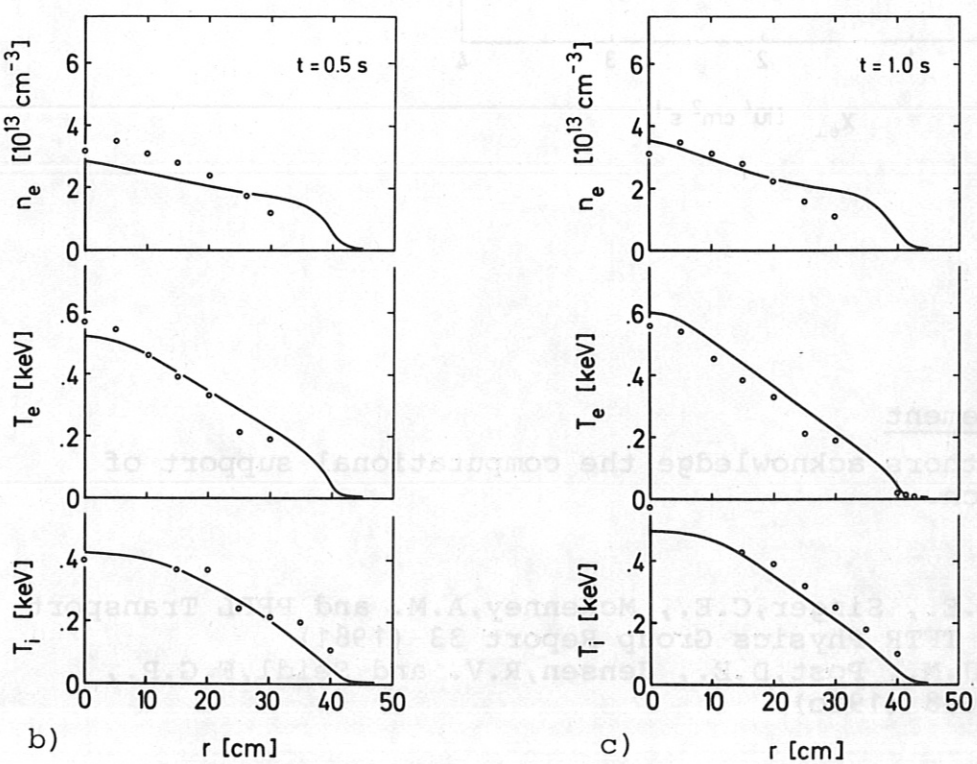

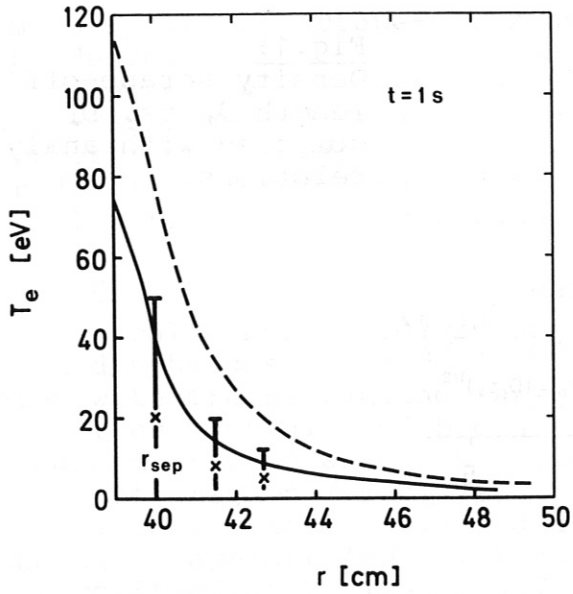

Fig.3:
Computed T_e-profiles in the scrape-off region with convection and heat conduction $\parallel \vec{B}$ (solid curve) and convection alone (dashed curve).

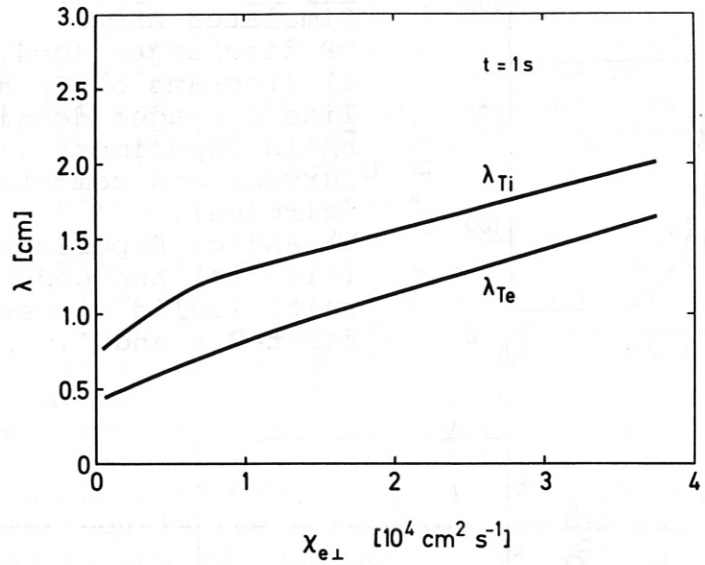

Fig.4:
Temperature scrape-off lengths λ_{Te} and λ_{Ti} vs. $\chi_{e\perp}$ with convection and heat conduction $\parallel \vec{B}$.

Acknowledgement

The authors acknowledge the computational support of R.Wunderlich.

References

/1/ Post,D.E., Singer,C.E., McKenney,A.M. and PPPL Transport Group, TFTR Physics Group Report 33 (1981)
/2/ Ogden,J.M., Post,D.E., Jensen,R.V. and Seidl,F.G.P., PPPL-1608 (1980)